ABSTRACT

Title of Document: ANALYSIS OF FLOW-BASED MICROFLUIDIC GRADIENT GENERATORS FOR THE STUDY OF BACTERIAL CHEMOTAXIS

Christopher James Wolfram, M.S., 2015

Directed By: Professor Gary W. Rubloff, Department of Materials Science & Engineering and the Institute for Systems Research

Chemotaxis is a phenomenon which enables cells to sense concentrations of certain chemical species in their microenvironment and move towards chemically favorable regions. This behavior is best understood in the bacteria *Escherichia coli,* which exhibits chemotaxis towards a variety of energy sources and signaling molecules. Recent advances in microbiology have engineered the chemotactic properties of bacteria to perform novel functions, but traditional methods of characterizing chemotaxis are not sufficient for such complex applications.

The field of microfluidics offers solutions in the form of gradient generators. Many of these gradient generators are flow-based, where a chemical species diffuses across a solution moving through a microchannel. A microfluidic gradient generator was explored as a chemotaxis platform. Sources of error during experimental operation and methods of mitigating this error were demonstrated, and the fundamental theory behind these devices was examined. These devices were determined to be inadequate for the study of bacterial chemotaxis.

ANALYSIS OF FLOW-BASED MICROFLUIDIC GRADIENT GENERATORS FOR THE STUDY OF BACTERIAL CHEMOTAXIS

By

Christopher James Wolfram

Thesis submitted to the Faculty of the Graduate School of the
University of Maryland, College Park, in partial fulfillment
of the requirements for the degree of
Master of Science
2015

Advisory Committee:
Professor Gary W. Rubloff, Chair
Professor William E. Bentley
Professor Isabel K. Lloyd
Professor Herman O. Sintim

Acknowledgements

I would like to extend my deepest thanks to my advisor Dr. Gary Rubloff, for his guidance at every step of this process and his understanding of the ups and downs of academic research, especially when that research delves into biology.

I am thankful for the encouragement I have received throughout my education from my family and friends, especially my fellow graduate student, Veronica.

I greatly appreciate the support of my committee members—Dr. Bentley and Dr. Sintim have been sources of endless ideas throughout this process, and Dr. Lloyd's counsel over the past six years, first as my undergraduate academic advisor, and now as a member of my thesis committee, has been invaluable.

Special thanks go to Dr. Xiaolong Luo, a Rubloff group alumnus who has given me direction throughout my graduate career and always found time to stop by the lab and help. My fellow group members have also provided assistance and insight along the way, for which I am very thankful.

I would also like to thank the members of the Bentley group and the Sintim group for their collaborative work on this project. Dr. Hsuan-Chen Wu's expertise in microbiology was especially helpful throughout this process. I also appreciate the support and feedback of all the members of the Biochip Collaborative.

The Maryland NanoCenter facilities made this work possible, and I would like to especially thank the FabLab staff for their training, expertise, and camaraderie.

This work was supported in part by the Robert W. Deutsch Foundation and by the NSF CBET program.

Table of Contents

List of Tables

List of Figures

Chapter 1: Introduction

This chapter will describe the phenomenon of bacterial chemotaxis, recent progress in engineering this behavior, and the most common methods that are used for characterizing chemotactic responses. It will then explain the motivation for developing microfluidic gradient generators as platforms for studying bacterial chemotaxis, and why the work detailed in this thesis is necessary for determining whether these platforms are viable.

1.1 Bacterial Chemotaxis

Bacteria, as some of the smallest and most numerous organisms on Earth, utilize a wide variety of mechanisms to ensure they both survive and flourish. When bacteria exist as freely-moving single cells, their patterns of movement and migration are crucial in ensuring they find a suitable microenvironment to sustain them and allow for cell division. Most bacteria are capable of directional migration through taxis, wherein they can respond to both positive and negative stimuli. Different bacteria species display many types of taxis for different forms of stimuli, such as aerotaxis, magnetotaxis, or phototaxis. However, the most common and well-understood form is chemotaxis—movement along a gradient of a chemical species, known as a "chemoeffector."

Chemotaxis enables bacteria to move to regions with high concentrations of food molecules or signaling molecules, in which case these chemical species would serve as chemoattractants, or to move away from regions with high concentrations of certain molecules which act as chemorepellents. The mechanisms of bacterial

chemotaxis are well-known. Several well-known publications have elucidated and explained the underlying mechanisms of chemotaxis[1–4]. Subsequent work added details such as to this understanding, and utilized new technologies such as super-resolution light microscopy and optical tweezers to visualize the chemotactic receptors on an individual bacterium and characterize the force generated by a single bacterium in response to a chemoeffector[5,6]. Microfluidic gradient generators offer novel, highly controllable platforms for the study of bacterial chemotaxis. Flow-based gradient generators in particular yield gradients that are stable over long periods of time, a highly useful property when examining bacterial behavior. However, experimental work and theoretical simulations are needed to demonstrate whether these platforms can successfully be used for this application. This thesis seeks to provide this information and an answer to whether flow-based microfluidic gradient generators are a viable method of characterizing bacterial chemotaxis.

1.2 E. coli Chemotaxis Signal Transduction

Escherichia coli is the most widely studied species of bacteria, and as a result its mechanisms of movement and chemotaxis are well understood and can be extrapolated to many other species of bacteria that also possess similar two component sensory systems. *E. coli* follows a "run-and-tumble" movement pattern, where a single bacterium travels in a straight line for several seconds, then changes direction and travels in another straight line[7]. The pattern is similar to the "random walk" patterns found in many scientific fields. It accomplishes this through the signaling pathway shown in Fig. 1-1, adapted from Grebe, et al.[8].

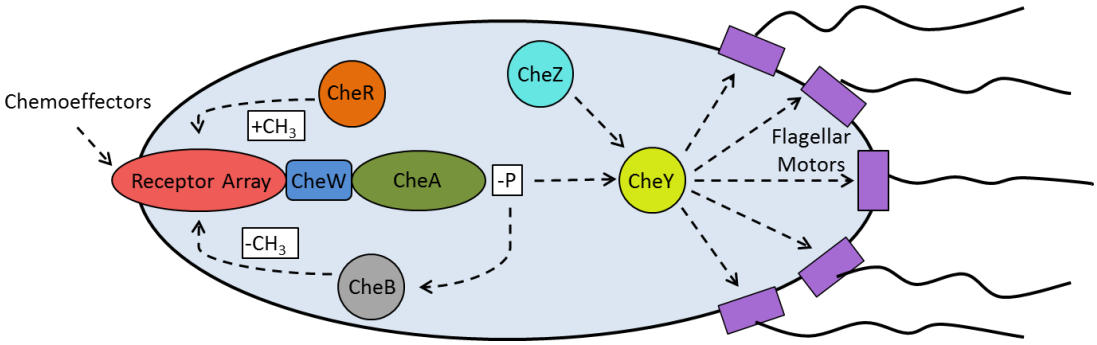

Figure 1-1. Diagram of the signal transduction pathways involved in *E. coli* chemotaxis[8].

E. coli use several flagella clustered on the cell membrane at one pole as a propulsion system. Each individual flagellum is a left-handed helix, so that when they rotate counterclockwise, the flagella form a coherent bundle that "pulls" the bacteria through its environment, allowing it to travel in a straight path. However, when the flagella rotate clockwise, the bundle is destroyed and the flagella push in different directions, causing the bacteria to "tumble." The direction of rotation is switched using a flagellar "motor" inside the cell membrane. When the protein CheY is phosphorylated, the resulting phospho-CheY complex diffuses through the cell and binds to the switch component of the flagellar motor. This causes the motor to rotate clockwise and the bacterium to tumble. When CheY is not bound to the flagellar switch, the flagella rotate counterclockwise and the bacterium "runs." While CheY will eventually naturally dephosphorylate through spontaneous self-hydrolysis, and subsequently unbind from the flagellar switch, the protein CheZ also dephosphorylates bound CheY, leading to a more rapid response to external stimuli.

While this mechanism explains bacterial motility, it does not address the process of chemotaxis. Chemotaxis is based upon a bacterium's ability to sense a change in the concentration of a chemoeffector as it moves along a gradient. In

response, the bacterium adjusts the frequency of tumbling events—when it is moving in a favorable direction (towards a higher concentration of a chemoattractant or a lower concentration of a chemorepellent) it will increase the lengths of its runs before it changes direction, and vice versa for unfavorable directions. This leads to a net movement in one direction, whereas in the absence of any gradients, the bacteria will simply follow a random walk pattern and no net movement is observed.

The understanding of chemotaxis signal transduction in *E. coli* that follows here is primarily derived from three well-known articles and papers, which provide in-depth and accurate descriptions of this process[8–10]. The second aspect of this process accounts for the ability of an *E. coli* bacterium to modulate its run length in response to the concentration of chemoeffector that it currently senses. When a bacterium encounters a chemoeffector molecule, the chemoeffector binds to one of several receptors on the cell membrane, as shown above in Fig. 1-1. Each receptor is specific to certain molecules, and is named according to the main molecules which each bind. The five receptors are Trg, which binds ribose and galactose; Tar, which binds aspartate; Tsr, which binds serine; Tap, which binds peptides, and Aer, which regulates aerotaxis through interacting with redox molecules. Trg, Tar, Tsr, and Tap are known as methyl-accepting chemotaxis proteins (MCPs). These receptors are linked to CheA, a histidine kinase, by the protein CheW. CheA autophosphorylates, even when not in the presence of a chemoeffector. However, when a chemoattractant binds to a receptor, the autophosphorylation rate of CheA decreases, whereas a chemorepellent increases the autophosphorylation rate[10]. Once CheA dephosphorylates, the phosphate group is transferred to either of the proteins CheY or

CheB. CheB, along with the protein CheR catalyze the methylation and demethylation of glutamyl residues in the cytoplasmic region of the receptors. CheY, as mentioned earlier, is responsible for binding to the switch of the flagellar motor[8]. When CheA autophosphorylates at a lower rate, such as when a receptor binds a chemoattractant, the phosphorylation rate of CheY also decreases. As a result, the frequency of phosphorylated CheY binding to the flagellar motor switch decreases and the overall frequency of tumbling events decreases as well, thus leading to longer run lengths.

There is a third component that is essential the bacterial chemotaxis process. While binding of an attractant or repellent induces changes in the frequency of tumbling events, and thus a change in the length of bacterial runs, bacteria must also be able to compare the concentration of a chemoeffector in their surrounding environment to the concentration they detected previously. This enables them to move towards the most favorable environments. For example, a chemoattractant may bind to a bacterium and increase the length of its run, but this could propel it towards a region of lower concentration of that chemoattractant; it needs to detect this decrease so it can move back towards the region of higher concentration, rather than simply decreasing its run length in response to the decreased concentration.

It achieves this through comparing the ligand occupancy of the receptors to the methylation state of the cytoplasmic region of the receptors[10]. The proteins CheB and CheR are essential to this process[11]. CheB, a methylesterase, demethylates the receptors when phosphorylated. CheR, a methyltransferase, methylates the receptors. In a region of constant concentrations of chemoeffectors, they will reach a steady-

state. The level of glutamate methylation of a receptor modulates its ability to stimulate CheA autophosphorylation. When an attractant binds to a receptor, it causes a decrease in the rate of CheA autophosphorylation as described earlier. This subsequently decreases the levels of phosphorylated CheY, which leads to fewer tumbling events and longer run lengths[11]. However, this also decreases the levels of phosphorylated CheB, while there is no change in the availability of CheR. Thus, CheB demethylates the receptors at a lower rate while CheR continues to methylate them, and the receptor is methylated more frequently, which then increases the rate of CheA autophosphorylation.

This adaptation mechanism leads to a temporary decrease in the rate of CheA autophosphorylation before it returns to the same rate it displayed prior to binding of the attractant. Conversely, when a receptor binds a repellent it will lead to an increase in the rate of CheA autophosphorylation and an increase in the phosphorylation of CheB, by the same process. The receptors will be demethylated more frequently, and the rate of CheA autophosphorylation will briefly increase before the increased demethylation activity of CheB restores the autophosphorylation rate to its pre-stimulus level. Thus, when a bacterium moves towards a higher concentration of an attractant, the receptor specific to that attractant will be occupied more frequently than the methylation of its glutamyl residues would indicate. The system is unable to adapt and CheA autophosphorylation will continue decreasing, sustaining the longer run lengths and decreased tumbling frequencies. The opposite will occur when moving towards a higher concentration of a chemorepellent.

This system of bacterial signal transduction is now well understood on a fundamental level, and has garnered significant attention in recent years as a target for novel genetic engineering to reprogram these behaviors and execute complex functions.

1.3 Novel Applications of Bacterial Chemotaxis

The most common examples of chemoeffectors are energy sources and nutrients, such as sugars and amino acids[12,13]. Bacteria use chemotaxis to move towards favorable environments, where a bacterial population can sustain growth for as long as possible. Bacteria also chemotax towards signaling molecules produced by other bacteria. This process is essential for quorum-sensing behavior, wherein bacteria detect the density of bacteria in their immediate environment through the concentration of these signaling molecules and execute a certain function above a threshold value. This mechanism, in turn, is what leads to the formation of biofilms, where bacteria produce and are embedded in a matrix of DNA, polysaccharides, and proteins.

Biofilms are significantly more resistant to antibiotics and other antimicrobial treatments than free-swimming bacteria, and biofilm formation often leads to chronic infections, the treatment of which is very difficult. Studying bacterial chemotaxis may eventually yield solutions to limit pathogenicity, reduce the length of infections in clinical settings, and mitigate biofilm formation[14–16]. For example, Yingxue, et al. prepared chemotaxis-deficient mutants of *Vibrio harveyi*, a species of bacteria that uses chemotaxis to locate and infect certain fish. Subsequently, the growth, motility, adhesion, and virulence of these bacteria were significantly decreased, compared to

non-mutated strains. Modulation of bacterial chemotaxis properties may open up new avenues for treatment of infections, thus slowing or halting the evolution of antibiotic resistant strains, an increasingly concerning aspect of modern healthcare.

However, there are additional possibilities of actually harnessing the bacterial chemotaxis mechanism to aid in a variety of functions. Bacteria are a biological prototype of a "microrobot" which can seek and follow environmental cues. In his landmark paper, "Life at Low Reynolds Number," E.M. Purcell focuses primarily on the motility and chemotaxis mechanisms of bacterial chemotaxis, as they serve as examples of both the challenges facing microscale robotics and possible means of overcoming them[17]. Recently, his speculations have become reality, as microbiologists now possess a diverse toolbox for reprogramming bacterial behaviors. Mishler et al. reviewed recent advances in engineering bacterial chemotaxis[18].Several papers are of special interest, since they demonstrate successful reprogramming of the chemotaxis pathway to perform new functions[19–21].

Hwang, et al. recruited the chemotaxis properties of *E. coli* to "seek and destroy" another pathogenic bacteria, *Pseudomonas aeruginosa*. *P. aeruginosa* secretes a signaling molecule, N-Acyl homoserine lactone (AHL), used in quorum sensing. A strain of *E. coli* was transformed such that CheZ is expressed in response to AHL. When *E. coli* lacks CheZ, it will continuously tumble and no chemotaxis or movement will occur. This mechanism enabled the transformed *E. coli* to move towards regions of higher concentration of AHL. This *E. coli* strain was also engineered with a plasmid that introduced an AHL-dependent quorum sensing mechanism, so that the *E. coli* execute a response above a certain threshold. This

response is the secretion of two substances, an antibiofilm enzyme to destabilize *P. aeruginosa* biofilms, and an antimicrobial peptide to kill the bacteria. This is one example of many chemotaxis-dependent genetic circuits that have been recently developed, and such complex systems demand characterization methods that can accurately demonstrate these finely-tuned properties.

1.4 Chemotaxis Characterization

The advent of these novel applications of engineered bacterial chemotaxis demonstrates how quickly the field of microbiology has advanced in the past decade. However, the development of methods for studying chemotaxis of a bacterial population has not kept pace with this progress. The ability to examine chemotaxis of a bacterial population as a function of time and environmental conditions, and in precisely-controlled chemical gradients, is fundamentally important to the continued development of these novel applications.

1.4.1 Capillary, Agar, and Transwell Assays

The capillary assay was one of the first assays used for chemotaxis[22]. In this procedure, a capillary tube containing a solution of the chemoeffector is submerged in a container of bacteria in media or buffer, as depicted in Fig. 1-2a.

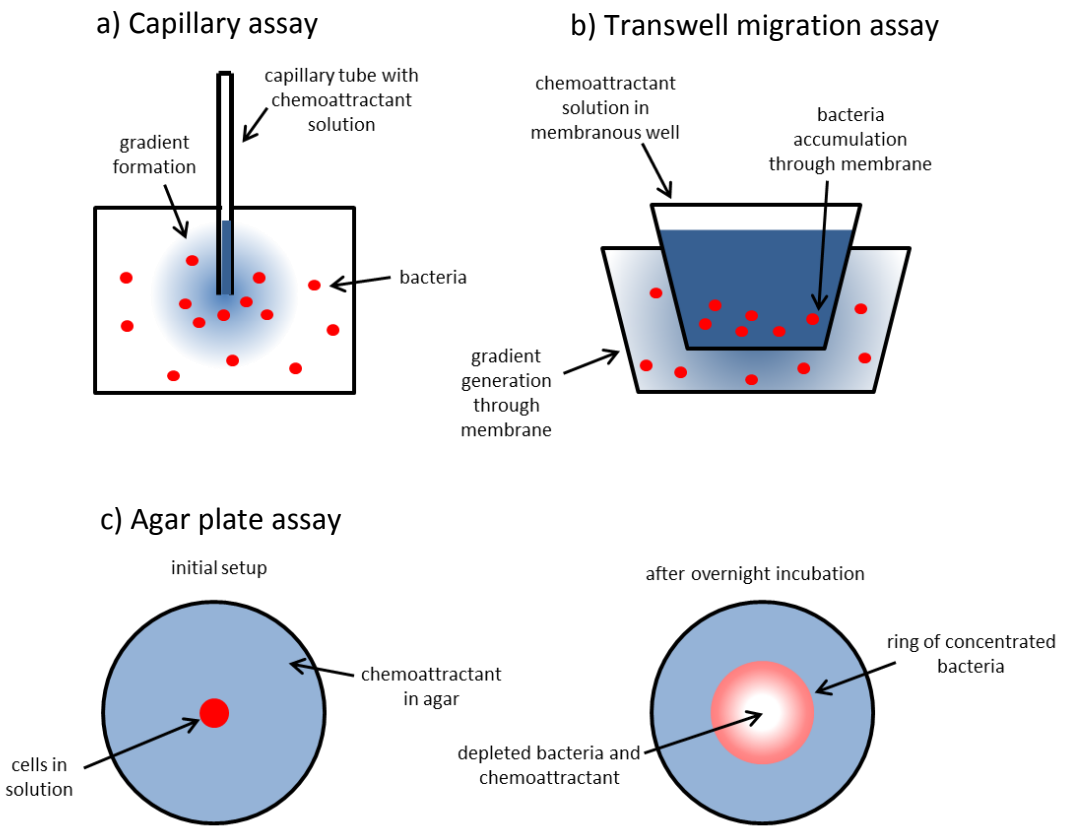

Figure 1-2. Traditional methods of characterizing bacterial chemotaxis. a) Capillary assay. b) Transwell migration assay. c) Agar plate assay.

After 30 minutes, the capillary tube is removed and the solution inside the capillary is applied to an agar plate. The number of colonies present after overnight incubation is then counted and this figure is used as the number of bacteria that migrated into the capillary. This method was successfully utilized to develop concentration ranges for the chemotactic response of *E. coli* to many of its known chemoeffectors, and to perform other fundamental studies[12,13,23]. However, reproducibility is difficult, and the assay itself is costly and labor-intensive.

An alternative method was outlined in 1975, using standard agar plates[24,25]. Agar is prepared normally, but combined with a chemoeffector of interest. The agar is then poured into a petri dish and allowed to cool. Finally, a small amount of bacteria

in solution is introduced at the center of the plate, and the plate is incubated at the optimal temperature for the desired time. If the chemoeffector is an attractant, the bacteria will migrate out into the agar, and as they consume the chemoattractant they generate a gradient which then leads to further migration outwards. Depending on the chemoattractant concentration and the time incubated, the bacteria will form visible bands, where they are most concentrated at the outer edge where the chemoattractant concentration is highest, and least concentrated near the center where it is lowest. This method is depicted in Fig. 1-2c.

This test, known as an agar plate assay, is advantageous over the previous capillary assay format, since the change in distribution of a bacterial colony is observed as a function of time. It is also simpler to prepare, and strains can be directly compared. While this method does not enable the study of chemorepellents, alternative formulations have been developed, where the bacteria are instead present in the agar, and the chemorepellent is introduced at the center of the plate. While this method is the standard used for simple evaluation of chemotactic responses, recent work has highlighted concerns about whether the patterns observed are actually the result of chemotaxis. Li, et al. prepared a strain of non-motile bacteria by knocking out the motB gene, which is required for flagellar rotation, but similar chemotaxis patterns appeared in response to the chemoattractant alanine[26]. A similar experiment resulted in the same phenomenon in mutants lacking a protein that leads to aflagellation, and in mutants lacking CheY[27].

While the reasons for this are not yet clear, it was theorized that the observed pattern may be build-up of a precipitate, rather than migration of the bacteria colony

itself [26]. Additionally, it can be difficult to control environmental factors between plates and to ensure that constant concentrations of chemoeffectors and bacteria are maintained across all experiments, and to ensure that external factors do not introduce error. However, this method is still one of the predominant methods used for basic tests of bacterial chemotaxis, and has been for over 30 years.

Another alternative method is the Transwell migration assay. This is similar to a capillary assay, but instead uses well plates with permeable supports. The chemoattractant solution is placed in these wells, and the plate is then assembled on top of another well plate which contains bacteria in solution. The wells with permeable supports are immersed in the bacterial solution, and a concentration gradient of the chemoattractant is generated through the support. The bacteria then migrate along the gradient and through the support into the upper well plate. After a defined time period, the top well plate is removed and the bacteria collected can be quantified. A schematic of this method is shown in Fig. 1-2b.

1.4.2 Microfluidic Gradient Generators

The advent of microfluidics technology has led to new technologies in many fields, but in biotechnology it is especially advantageous. The small sample volumes and high throughput lend themselves well to diagnostics, and the easy-to-fabricate and disposable nature of microfluidic devices is one of the cornerstones on which the current growth in lab-on-a-chip platforms rests. Fluids exhibit very different properties on the microscale than on the macroscale, and these differences can be

harnessed to precisely control the microenvironment experienced by small organisms, such as bacteria.

A common application of microfluidics is precise generation of gradients of chemical species. The simplest iteration of such a device, with an example of a typical chemical gradient generated, is shown in Fig. 1-3.

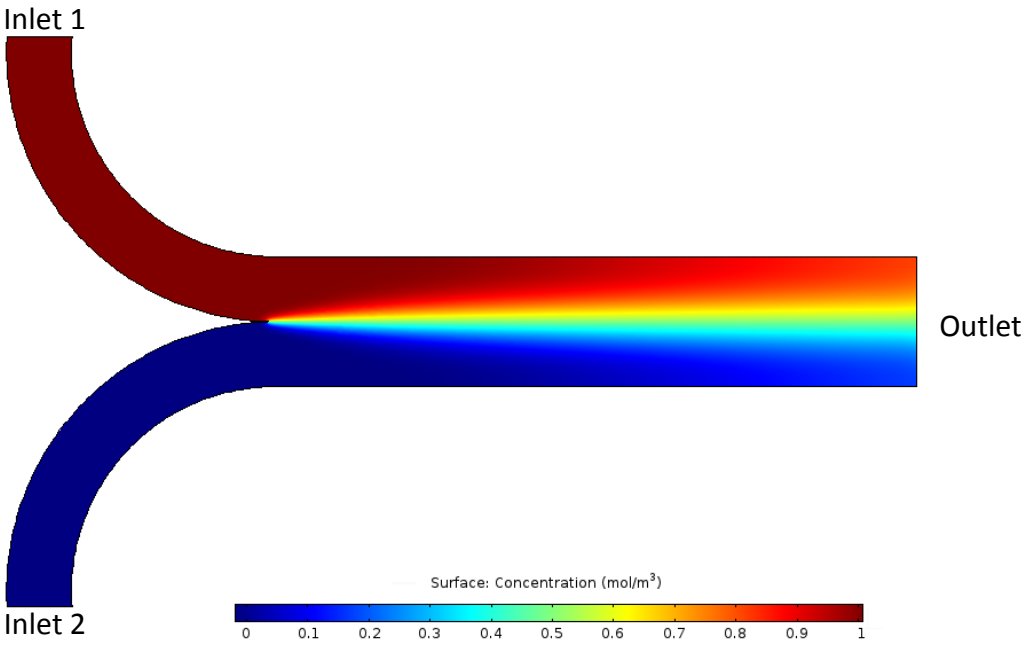

Figure 1-3. A simple two-inlet microfluidic gradient generator, simulated using COMSOL multiphysics software. The diffusing molecule has a molecular weight of 180.1559 g/mol (the molecular weight of glucose), and the flow rate through each individual inlet is 1.0 μL/min.

The channel dimensions of such a small device cause the liquid in the channel to exhibit laminar flow, wherein the solutions in the channel flow in layers that do not mix, and experience different velocities due to friction from the channel walls or adjacent fluid layers. Thus, the chemical species injected into Inlet 1 will diffuse across the interface between the two solutions and create a gradient which becomes smoother as the solutions travel farther down the channel. The concentration gradient across the channel width follows a Boltzmann distribution. Later research has yielded

more complex architectures, such as that shown in Fig. 1-4, to create smoother and more linear gradients. This particular device design is widely used in microfluidics for a variety of applications, including monitoring zebrafish development, differentiating Schwann-like cells by optimizing properties, and analysis of photodynamic therapy drugs through precise manipulation of a wide range of microenvironment factors[28–30].

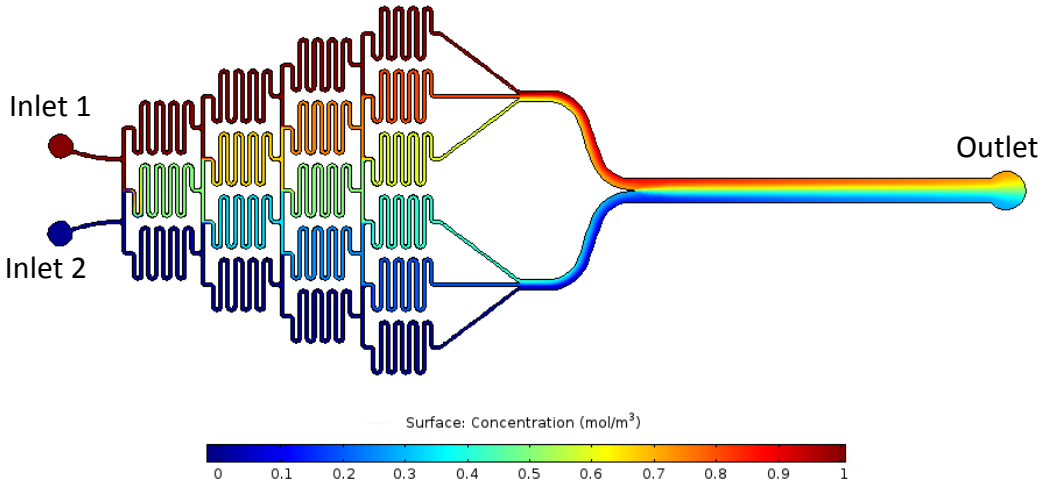

Figure 1-4. A complex two-inlet microfluidic gradient generator, where mixing occurs via a series of micromixers, simulated using COMSOL multiphysics software. The diffusing molecule has a molecular weight of 180.1559 g/mol (the molecular weight of glucose), and the flow rate through each individual inlet is 1.0 μL/min.

Several alternatives to flow-based microfluidic gradient generators have been developed. These typically rely on diffusion from a source and a sink into a main channel or chamber in which the bacteria can chemotax. The connections between the main chamber and the source and sink are normally porous membranes through which the chemical species can diffuse. An example of one of these devices developed by Diao et al., is shown in Fig. 1-5[31].

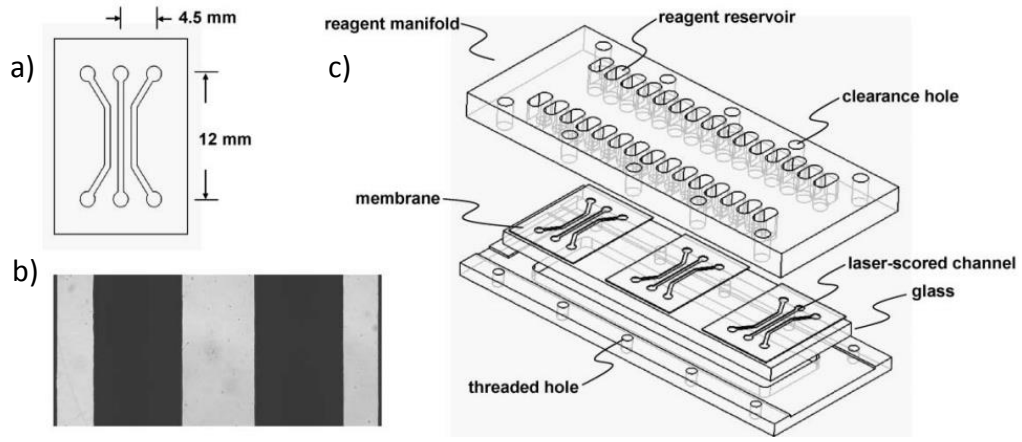

Figure 1-5. A membrane-based gradient generator, where the cells are in a non-flowing, static environment. a) Top-down view of the device, where the channel cutouts are fabricated from a porous nitrocellulose membrane. b) Micrograph of the channels in a fabricated device. c) Schematic of the full device, where the membranes are inserted between a polycarbonate manifold and a glass slide. Reprinted with permission from *Lab on a Chip*, 2006, **6**, 381-388[31].

The advantage of these platforms is that the bacteria can move through a static environment, so that flow does not suppress or otherwise modulate their chemotactic response. Additionally, it can be easier to track a single bacterium over time, since they are not being rapidly displaced. However, these devices are less able to generate precisely controlled gradients, since the concentrations depend on the membrane and chemoeffector properties, the device geometry, and the time allowed for the gradient to form. Additionally, the gradient will eventually decay with time, and the concentration range cannot be precisely defined as in flow-based gradient generators. At first glance, it seems that flow-based gradient generators offer several advantages that make them a superior choice for the study of the complex bacterial chemotaxis mechanism. The following work is a detailed exploration of this application, and both experimental and theoretical complications present in flow-based microfluidic gradient generators.

Chapter 2: Materials & Methods

2.1 Mold Fabrication

Table 2-1: Master mold fabrication process for device schematic shown in Fig. 3-1.

Step	Parameters
1. master mold substrate selection	100 mm silicon wafer
2. wafer cleaning	rinse with acetone, methanol, isopropanol, and deionized water
3. dehydration bake	120°C for 1 hour
4. photoresist selection	SU-8 50 negative photoresist at room temperature
5. spin coating	50 μm thickness: 100 rpm/sec ramp to 500 rpm for 10 seconds, 200 rpm/sec ramp to 2000 rpm for 30 seconds
6. soft bake	65°C for 10 minutes, 95°C for 30 minutes, room temperature for 5 minutes
7. mask properties	printed on mylar transparency, taped to transparent quartz plate
8. exposure	27 mJ/cm2 energy mask aligner, 30 intervals of 0.5 second exposure time with 15 second pause between intervals, total exposure dose of 600 mJ/cm2
9. post bake	room temperature for 5 minutes, 65°C for 5 minutes, 95°C for 15 minutes
10. development	SU-8 developer for approximately 5 minutes (until only exposed pattern remains)
11. hard bake	150°C for 5 minutes

Microfluidic devices were fabricated using a standard soft lithography molding approach, where polydimethylsiloxane is molded against photoresist-patterned silicon wafers. Mask designs were drawn using AutoCAD 2014 software, and these drawings were printed on Mylar transparencies by CAD/Art Services. 100 mm single side-polished silicon wafers were purchased from University Wafer. Wafers were cleaned using a series of acetone, methanol, isopropanol, and deionized water rinses, then

gently dried with N_2. This was followed by a dehydration bake on a 120°C hotplate for one hour.

SU-8 50 negative photoresist and SU-8 developer were purchased from MicroChem. SU-8 50 was stored in a refrigerated environment, and allowed to warm to room temperature for two hours prior to use. A Laurell Spin Coater, model WS-650MZ-23NPP, was used to coat SU-8 50 photoresist on silicon wafers. The wafer was placed on the spin coater vacuum chuck, vacuum was applied, and SU-8 50 was dispensed to cover approximately 2/3 of the wafer surface. The spin coater was programmed to ramp up at 100 rpm/sec to 500 rpm for 10 seconds, and then ramp up at 200 rpm/sec to 2000 rpm for 30 seconds. This yields a final photoresist thickness of approximately 50 μm. The wafers with spun photoresist were then removed from the spin coater and underwent a soft bake on a 65°C hotplate for 10 minutes before being transferred to a 95°C hotplate and soft baking for another 30 minutes.

Microchem's instructions state that for this thickness, a soft bake of 6 minutes and 20 minutes at the respective temperatures is sufficient; however, it was found that increasing the soft bake time helped improve the resolution of the final structures and minimize cracking in the photoresist surface. Following the soft bake, the wafers were removed from the hotplate and allowed to cool for 5 minutes before exposure. The exposure was performed using an EVG 620 Mask Aligner, with energy of 27 mJ/cm^2. The Mylar transparencies were taped to a quartz plate and positioned in the instrument so that the printed side of the transparency was adjacent to the wafer, to minimize light diffraction between passing through the printed mask and exposing the photoresist.

The total exposure dose was increased from Microchem's recommended amount of 400 mJ/cm^2 for this thickness to 600 mJ/cm^2, since it was found that this yielded cleaner structures with minimal surface cracking of the photoresist. Additionally, the exposure was performed in intervals of 0.5 seconds, with 15 seconds of rest in between (approximately 15 total seconds of exposure, and 7 minutes, 45 seconds total runtime). This aided in obtaining clean structures as well, since long exposures can heat the surface of the silicon wafer. This heating can cause a hard crust to form on top of the photoresist, which can decrease the amount of light that passes through the photoresist. Since photoresist closer to the wafer surface will be underexposed, this can lead to uneven structure features after development, or complete detachment of features from the wafer surface.

The wafers were then removed from the mask aligner and allowed to sit at room temperature for 5 minutes, to allow crosslinking to occur. This was followed with a post bake at 65°C for 5 minutes and 95°C for 15 minutes, again increased from Microchem's recommendation of 1 minute and 5 minutes respectively, due to the reasons described for the soft bake. Finally, wafers were developed in SU-8 developer for approximately 5 minutes, rinsed with isopropanol and DI water, and dried with N_2. Finally, the wafers were hard baked at 150°C for 5 minutes to ensure good adhesion and minimize surface cracking.

2.2 Device Fabrication

Table 2-2: Device fabrication process for device schematic shown in Fig. 3-1.

Device Fabrication Process
1. PDMS elastomer prepolymer and curing agent mixed in 10:1 ratio for total mass of 45 g
2. PDMS mixture degassed under vacuum for ~2 hours
3. PDMS mixture poured over master mold in petri dish
4. PDMS mixture on silicon wafer cured at 65°C for 2 hours
5. Cured PDMS peeled from master mold and individual devices cut from block
6. 25 mm x 75 mm glass slides rinsed with acetone, methanol, isopropanol, and deionized water, and dehydrated at 120°C for 30 minutes
7. PDMS devices and glass slides plasma treated at 450 mTorr pressure, 20 W, 20 sccm O_2, for 30 seconds
8. PDMS and glass slides bonded together to form final device

PDMS devices were prepared following completion of the silicon master molds. Dow Corning Sylgard 184 silicone elastomer kits were purchased from Ellsworth Adhesives. PDMS was mixed in a 10:1 ratio of prepolymer:curing agent. The resulting liquid PDMS mixture was degassed under vacuum, then gently poured over the silicon master mold inside a plastic petri dish. The PDMS was cured in a 65°C oven for 2 hours or until solid, allowed to cool, and peeled off the silicon master mold surface. The PDMS was cut with a razor into defined devices, and inlets and outlets for tubing were reverse-punched using a 1 mm tissue biopsy punch.

25 mm x 75 mm glass slides were rinsed using acetone, methanol, isopranol, and DI water, then dried under N_2 and placed on a 120°C hotplate for 30 minutes. Oxygen plasma treatment with a Branson Barrel Resist Stripper was used to irreversibly bond the PDMS devices to the glass slides. The PDMS layer and the glass slide were placed in the resist stripper with the sides to be bonded together placed facing the plasma, and exposed to plasma at 450 mTorr pressure, 20 W, 20

sccm O_2, for 30 seconds. After removal, the PDMS and glass slide were placed into contact and a permanent bond was formed. The devices were then allowed to rest overnight for the bond for the PDMS surface to recover its hydrophobicity.

2.3 Cell Preparation

A fluorescent strain of *E. coli* was prepared using standard protocols. *E. coli* K-12 W3110 (ΔlsrFG ΔluxS) was transformed with the plasmid pET-DsRed_tac-ompA-proteinG to yield cells which express *Discoma sp.* red fluorescent protein (DsRed) on their surface[21]. Bacteria cultures were grown overnight in Luria-Bertani broth, containing 5g of yeast extract per liter, 10 g of Bacto tryptone per liter, and 10 g of NaCl per liter[32]. Cells were incubated in Erlenmeyer flasks at 30°C with shaking at 250 rpm. Cultures were then centrifuged at 12,000 rpm for 10 minutes in a microcentrifuge. The cleared supernatant was removed, and the cells were dispersed in D-PBS with an optical density of 0.6.

2.4 Device Operation

Microfluidic devices were imaged in a Zeiss Axio Observer Z1 microscope, capable of both bright field and fluorescent image acquisition. An environmental chamber mounted on the microscope maintained a temperature of 37°C during operation, the optimal temperature for *E. coli*, to ensure maximum motility. Kent Scientific Genie Plus syringe pumps were used to introduce solutions into the device, through 1 mm outer diameter tubing. Flow rates were varied, with a minimum of 0.1 μL/min through each individual inlet, for a total flow rate of 0.2 μL/min in the device in the case of two inlets only, or 0.3 μL/min for three inlets. When using a

downstream cell inlet, as will be later described in 3.2, the flow rates were scaled appropriately for the width of each channel. The width of the cell inlet channel was 100 μm, and the width of the two channels that feed into the main channel was 600 μm each. Thus, when the flow rate through the two upstream inlets was 1 μL/min, the flow rate through the cell inlet was 0.17 μL/min. Concentration gradients were visualized with 1 mM fluorescein in deionized water. Chemotaxis solutions were prepared using D-glucose at a variety of concentrations in PBS as a chemoeffector solution, and PBS as a non-chemoeffector solution. Cell adhesion was tested by dispersing cells in solutions of LB media and D-PBS, introducing the cells in microfluidic channels, and rinsing with 1 mL of PBS after 5 minutes. BSA pretreatment of PDMS surfaces for the prevention of cell adhesion was performed by filling the microfluidic device with 2 mg/mL BSA, resting at room temperature for 10 minutes, and gently rinsing with 1 mL of PBS. The cells were then introduced and visualized using a fluorescent microscope to observe adhesion during flow.

Bubble formation during filling of the microfluidic device was a significant impediment to establishing precise gradients. This was prevented by first flowing PBS in through the outlet of the device at a high flow rate. This filled the channels completely with liquid, and by introducing it at the outlet, the rate at which the PBS travels into the micromixers is constant across the device, which prevents air being trapped between liquid interfaces. The high flow removes any bubbles that do form, either by detaching them from the PDMS walls and pushing them out of the channels with the flow, or by generating high pressure in the device that causes the air bubble to dissipate through the gas-permeable PDMS.

Chapter 3: Device Design

Flow-based microfluidic gradient generators are a novel solution to the lack of highly-controllable platforms for control of bacterial microenvironments and demonstration of resulting chemotaxis behavior. A review of the literature indicates that the most common microfluidic gradient generator design is that of the splitting and recombining micromixers. In this design two solutions, one with and one without a certain concentration of a molecule, are divided and combined by a pyramidal configuration of micromixers, such that when they recombine into one channel they form a linearly increasing concentration gradient. Indeed, this device has already been applied to the study of bacterial chemotaxis. In this chapter, the design of such a device is explored, with a focus on inlet configurations and the geometry of the main channel.

3.1 Device Design Background

A flow-based gradient generator was developed based on the design of Englert, et al. [33]. This design incorporates three inlets for solution, as shown in Fig. 3-1.

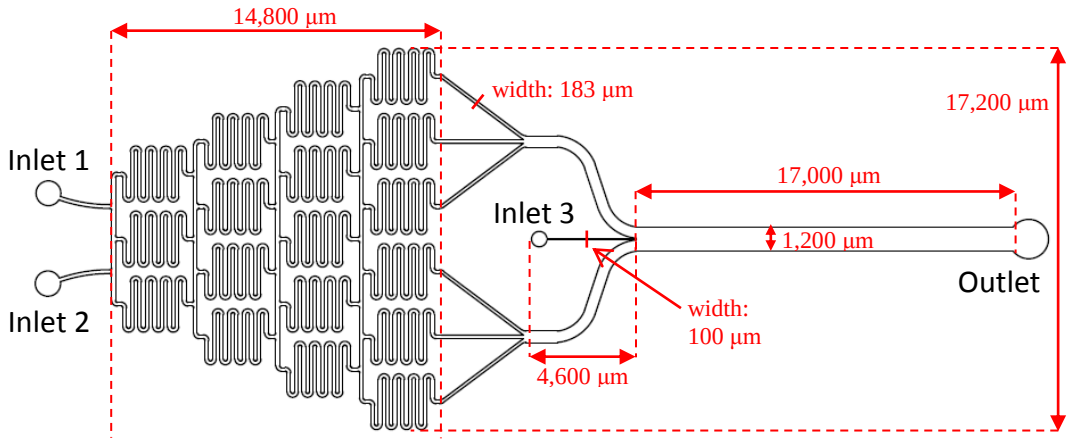

Figure 3-1. Device design featuring a downstream cell inlet, where inlet 1 introduces a solution containing a chemoeffector, inlet 2 introduces a buffer solution without any chemoeffector, and inlet 3 introduces cells in media or buffer. The channels in the micromixer array have a width of 183 µm each, and the cell inlet has a width of 100 µm.

Note that this device design differs slightly from that of Englert, et al. in dimensions and geometry, but the overall mechanisms and properties are identical. Here, inlet 1 introduces buffer, and inlet 2 introduces a chemoeffector solution. Inlet 3 is downstream and introduces a solution of cells in buffer or media. The buffer and chemoeffector solutions flow through a series of splitting and recombining serpentine micromixer channels, which generate six final concentrations of chemoeffector, distributed at regular intervals from 0 M to the concentration of the chemoeffector solution. For example, for a chemoeffector solution with a concentration of 1 mM, the six channels would have concentrations of 0.0 mM, 0.2 mM, 0.4 mM, 0.6 mM, 0.8 mM, and 1 mM. The channels then recombine and flow into a main channel, where the cell inlet introduces a cell population in the center of this gradient. As the solutions continue to flow down the channel, the gradient becomes smoother and the cells should be able to chemotax up the gradient of a chemoattractant or down the gradient of a chemorepellent.

3.2 Inlet Configuration

The introduction of the solution of cells at the downstream inlet, where the channels recombine to form the main channel, can be problematic due to fluctuations in the flow, either from the mechanism of operation of the syringe pumps or pressure variations in the device. This is described in more detail in 4.2. Given these factors, a variation of this design was explored where the cells are introduced at the same point as the buffer and chemoeffector solution, in a design shown in Fig. 3-2.

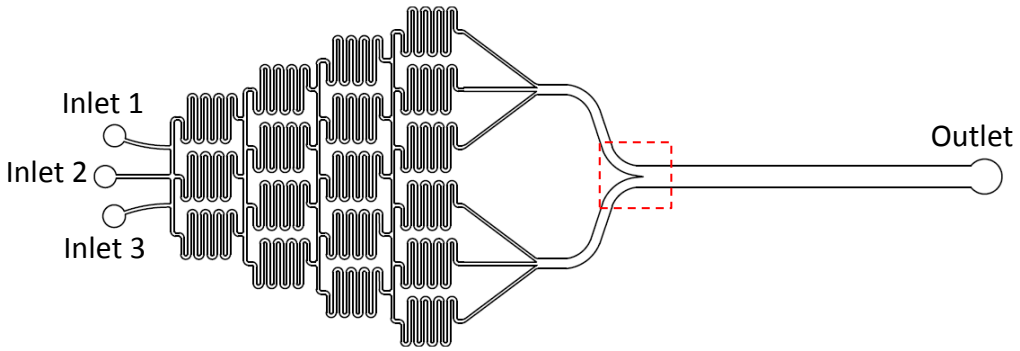

Figure 3-2. Device design featuring an upstream cell inlet, where inlet 1 introduces a solution containing a chemoeffector, inlet 2 introduces cells in solution, and inlet 3 introduces a buffer solution without any chemoeffector. The cells participate in the mixing, but in theory should generate a distribution that is symmetrical along the main channel length, with the highest concentration of cells at the center of the channel, and a decreasing concentration towards the channel side walls. The dashed red rectangle indicates the section of the device shown in Fig. 3-3.

The fundamental issue with this solution is that the cells are able to chemotax throughout the micromixers, which may result in variations in the distribution of the cell population once they are introduced to the main channel. An example of this is shown in Fig. 3-3a. Fig. 3-3b shows a corresponding fluorescence intensity profile across the channel width, while Fig. 3-3c shows the fluorescence intensity profile across each of the six individual channels just prior to joining together. The increase in fluorescence intensity is present before the cells enter the main channel, indicating

that what may look like chemotaxis in the main channel in the image was actually the result of either chemotaxis occurring in the micromixers or other sources of error.

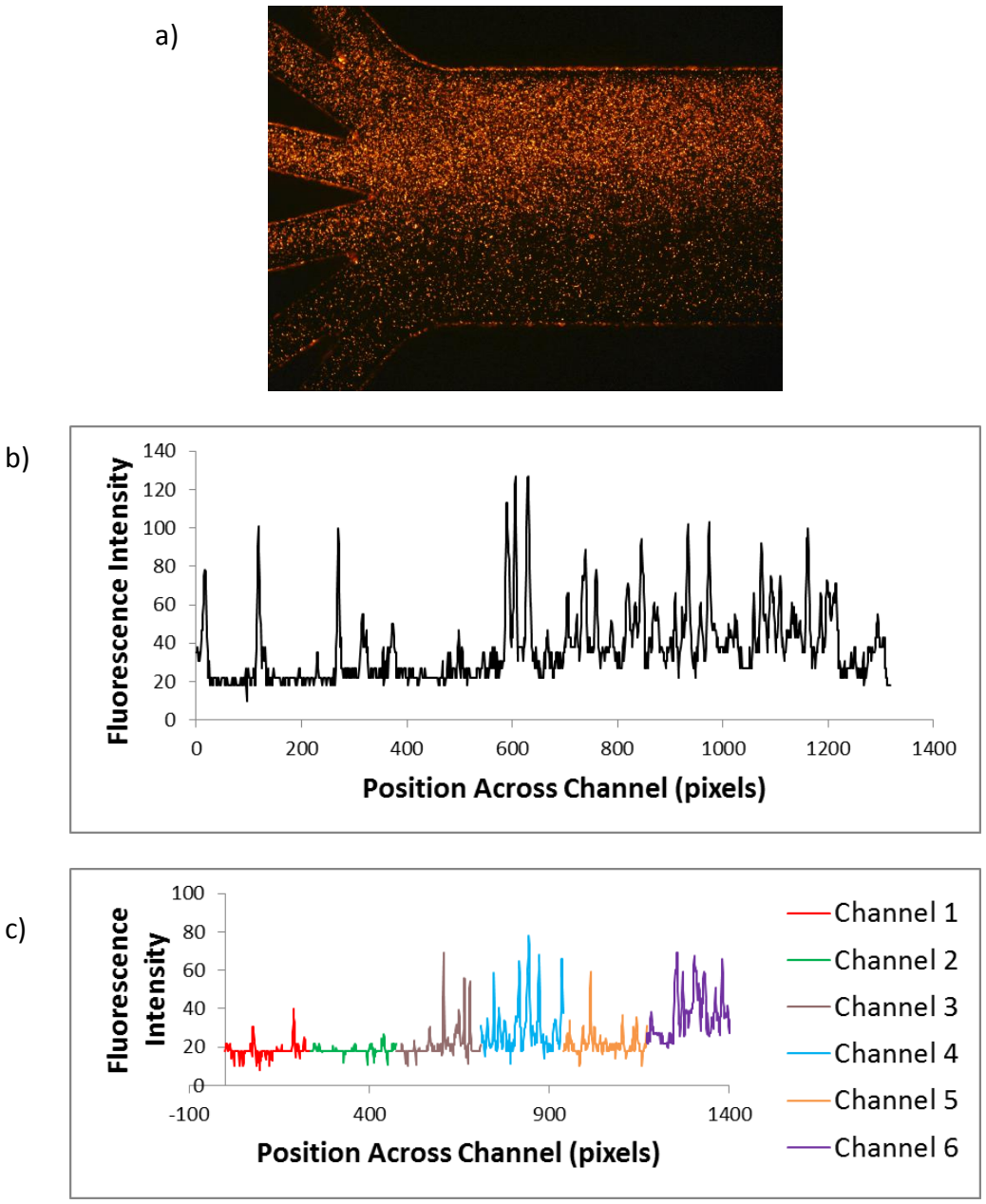

Figure 3-3. Image and analyses for device design featuring an upstream cell inlet, corresponding to the location inside the red dashed line in Fig. 3-2. It should be noted that for the purpose of analysis, an alternate device design was used, where 6 channels from the micromixer array remain separated until rejoining at the main channel. a) Fluorescent E. coli distribution in a microfluidic gradient generator, seemingly displaying chemotaxis. Brightness and contrast of this image were increased for visibility. b) ImageJ analysis of the fluorescence intensity across the channel width at the beginning of the main channel. c) ImageJ analysis of the fluorescence intensity in each individual feeder channel, immediately prior to rejoining to form the main channel.

While there are concerns with both device designs, it was found that the original design with the downstream cell inlet may be more desirable, simply because the issues described earlier are more easily visualized if they happen. When using the design with the upstream cell inlet it may be difficult to determine whether chemotaxis occurs in the micromixers, or if variations in cell distributions are attributable to other unknown factors.

3.3 Narrowing Main Channel

In 2.4, a method for preventing formation of bubbles while filling the device is described but the device design can also be altered to in eliminating bubbles after they are present. This is accomplished by increasing the pressure in the device so that the solution flow forces the bubbles out. However, this needs to be accomplished without changing the design so significantly that it affects the overall function or dimensions. Narrowing a small segment of the main channel near the outlet will increase the pressure in the channel, which will in turn exert pressure on any air bubbles present in the device, forcing air through the gas-permeable PDMS.

The pressure is determined from the Navier-Stokes equation:

$$\rho\left(\frac{\partial u}{\partial t} + u \cdot \nabla u\right) = -\nabla p + \mu\nabla^2 u + f_b$$

which is essentially a form of Newton's 2nd Law, $F = ma$, that is specific to fluid flow[34]. Fig. 3-4 shows a COMSOL simulation of the pressure in a microfluidic channel of width 1000 μm, with and without narrowing to a width of 200 μm. The pressure in the channel that narrows near the outlet is significantly higher, and is

continuous throughout, whereas in a channel of constant width the pressure is much lower and decreases gradually down the channel length.

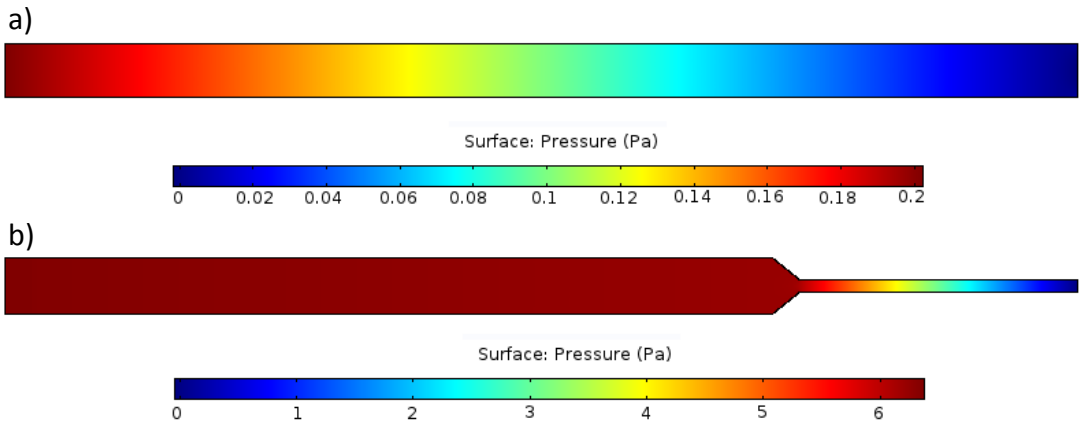

Figure 3-4. COMSOL multiphysics simulations of the pressure in the main channel. a) A main channel design where a constant width of 1000 μm is maintained. b) A main channel design where the channel width decreases to 200 μm.

However, it should be noted that this increase in hydrostatic pressure may have a significant effect on the cells, and further experimentation is needed to determine whether this will attenuate their ability to chemotax or function normally.

Chapter 4: Experimental Operation

This device, while simple in design, requires a significant amount of troubleshooting for consistent and accurate operation. This chapter will examine experimental issues that arise with this platform, namely the formation of bubbles, fluctuations in the flow, a non-linear gradient shape, the introduction of a local increasing gradient in both directions at the cell inlet, concentration optimization, and bacteria adhesion on the channel walls. Where possible, solutions are explored; when no solutions are clear, the impact on the device's operation is noted.

4.1 Bubble Formation

An additional concern with this device design is the introduction of bubbles and difficulties in removing them from the device. Bubbles form very easily in this device, since it is difficult to precisely control the flows from the two upstream inlets as they fill the micromixers. A bubble will form if a downstream channel fills with solution from one inlet while it is still filling with solution from the other inlet at a point upstream. Air is trapped between the two solutions, as illustrated in Fig. 4-1.

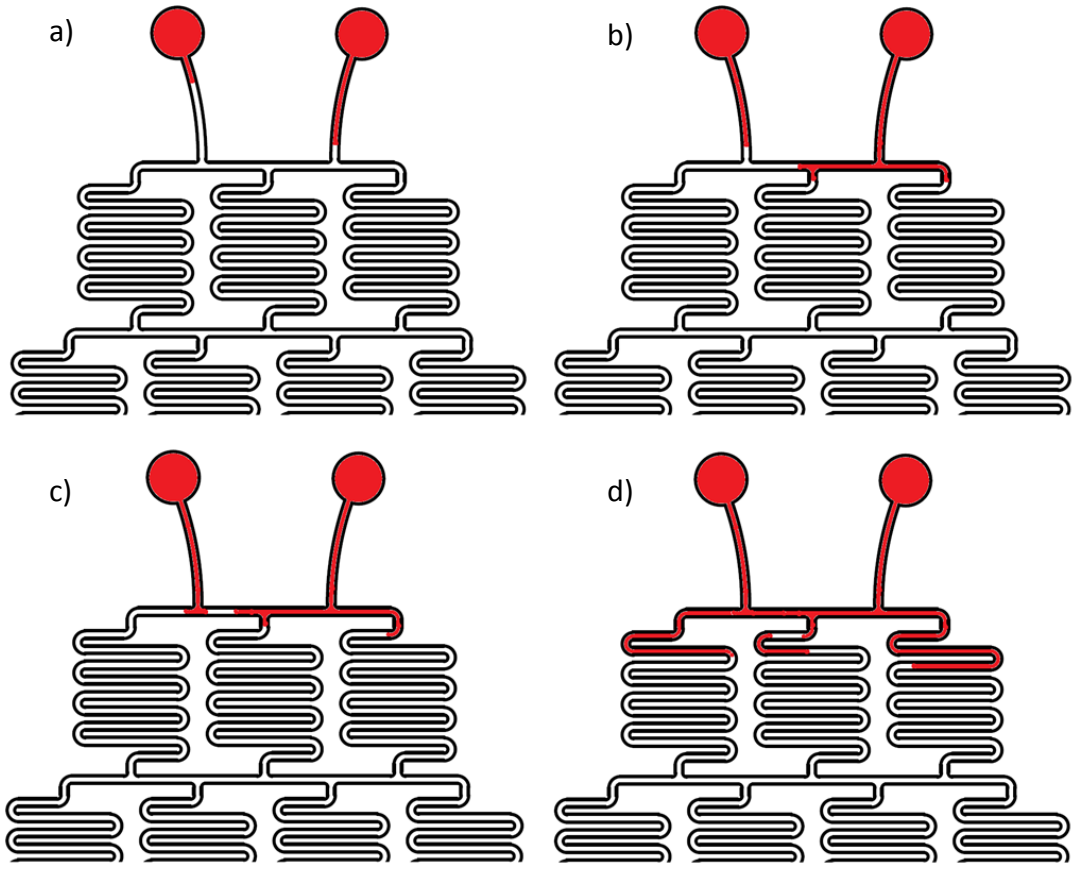

Figure 4-1. Schematic of bubble trapping due to uneven filling. a) The solutions flow into the two inlets at uneven rates. b) The solution flowing in more quickly begins to fill the micromixer array, flowing towards the other inlet simultaneously. c) A small pocket of air is trapped between the two solutions. d) The bubble is forced into the micromixer array, where it may become trapped or flow to the main channel and attach to the PDMS sidewalls. It should be noted that this effect will also cause the micromixers to continue to fill unevenly, creating more bubbles.

This can result in the solutions flowing to other micromixers, if the bubble is large enough that it requires more pressure to push it downstream than it would to alter the flow. This, in turn, can affect the gradient formation by causing uneven mixing of the two solutions. However, smaller bubbles will be forced through the micromixers and eventually arrive in the main channel. Examples of bubbles formed in the device are shown in Fig. 4-2.

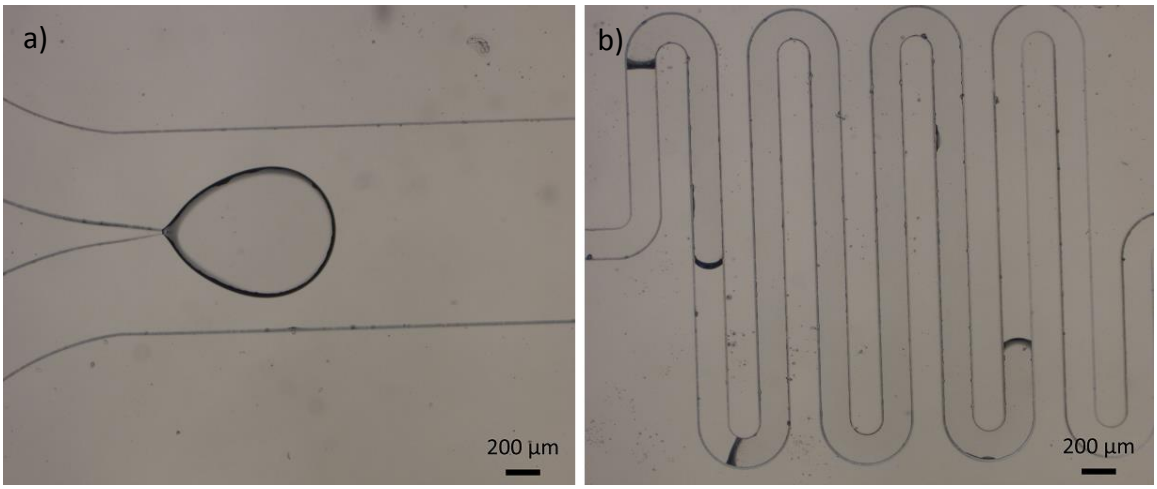

Figure 4-2. Images of bubbles trapped in a microfluidic device. a) A large bubble trapped at the junction of the two feeder channels and the main channel. b) Two bubbles trapped in a micromixer.

Due to the hydrophobic nature of PDMS and the large width of the main channel, bubbles may flow down into the main channel and become trapped on the side walls of the main channel. These bubbles can be extremely difficult to remove, since they "stick" to the hydrophobic PDMS surface, and are usually small enough that they do not fill the entire channel width, preventing them from being pushed out by flow. These bubbles can obstruct flow and interfere with the stability of the gradient, as shown in Fig. 4-3.

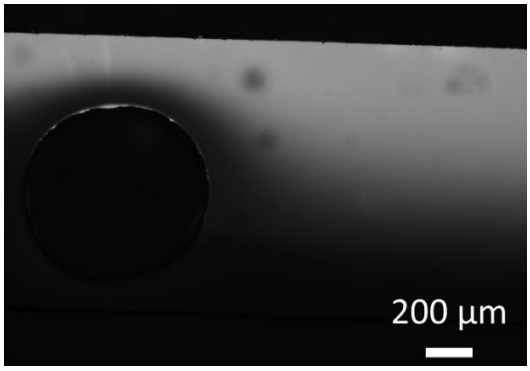

Figure 4-3. The distribution of a fluorescein gradient in the main channel as it flows past a large bubble. While the gradient is not destroyed, it fills the solution at an angle, creating a more uneven gradient. Additionally, since this bubble is in the center and not on the side of the channel, this behavior occurs on both sides of the bubble, and a sharp interface is created between the two sides when they rejoin.

In scenarios such as this, the flowing solutions usually do not push the bubbles through the channel to the outlet, and instead flow around the bubble as pictured. This can significantly affect the gradient, since this generates transversal flows that induce turbulent mixing and flattens the gradient, as shown in Fig. 4-4. Line profiles of the concentration gradient were taken before and after flowing past the bubble. The gradient before the position of the bubble was identical in both cases, but the gradient deteriorated by a larger degree after flowing past it.

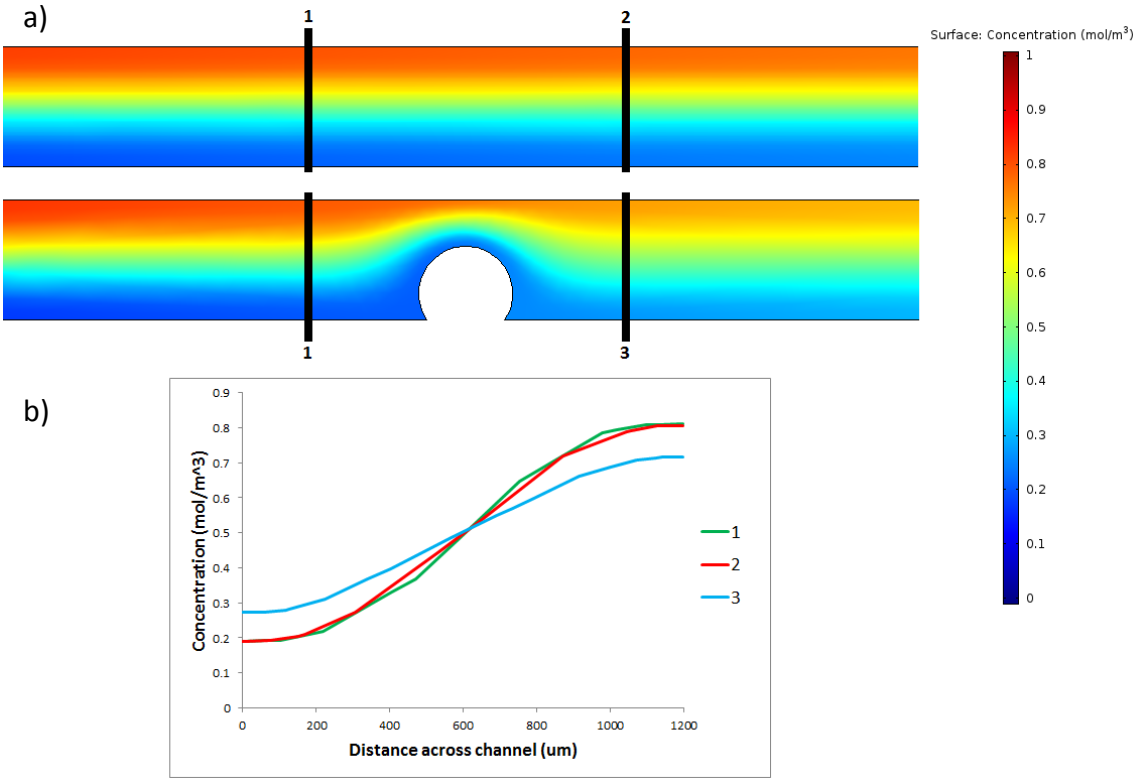

Figure 4-4. The effects of a bubble on the gradient in the main channel. a) COMSOL multiphysics simulations of a concentration gradient of glucose at a total flow rate of 2 μL/min through the device, without and with a bubble on the side wall. b) Plot of concentration gradients corresponding to labeled cut lines shown above, where the gradient is the same before the bubble, but decays significantly more after passing it.

These transveral flows may also significantly alter the position of cells, reducing or altogether eliminating their ability to accurately sense the gradient at that point, since they experience a large shift in position across the channel width. Bubble

formation can be addressed through pre-wetting the device, by flowing buffer in through the outlet. Filling the device in reverse from a single inlet (in this case the outlet) ensures that the micromixers fill simultaneously to minimize bubble formation. Additionally, if bubbles do form during this step the flow rate can be manually increased so that the high pressure forces the bubbles down the channel and through the outlet, or forces them to dissipate through the gas-permeable PDMS. Once the entire device is filled, enough buffer is introduced to form a droplet on the surface of each inlet. Then, the appropriate solutions can be introduced to the device by ensuring that a small droplet of each solution is found at the tubing entrance before inserting the tubing in the inlet. This additional step further minimizes bubble formation by bringing the two liquid interfaces into direct contact and preventing any bubbles being trapped between the solutions and the buffer filling the channel. The device geometry can also be changed to aid in bubble removal through increasing pressure in the main channel, as discussed in 3.3.

4.2 Flow Fluctuations

Flow fluctuations are also a significant challenge in the operation of this device, especially when using the device design with a downstream cell inlet, as discussed in 3.2. The introduction of flow at this point, in conjunction with the small width of the inlet relative to the large overall width at that point, can lead to the cell solution pushing back into the side channels instead of flowing linearly forward, or conversely, the solutions exiting the side channel can push back into the cell inlet. This was typically observed after the device had reached a steady-state, and at low flow rates. This may be due to the mechanism by which syringe pumps typically

operate. The pump depresses the syringe a fixed amount, and then pauses for an interval defined by the programmed flow rate. Due to this, if the three pumps are not operating so that the periods of depressing the syringe plunger are closely synced, the flow from the cell inlet can fluctuate to either side of the channel as shown in Fig. 4-5, obscuring any observed chemotactic response.

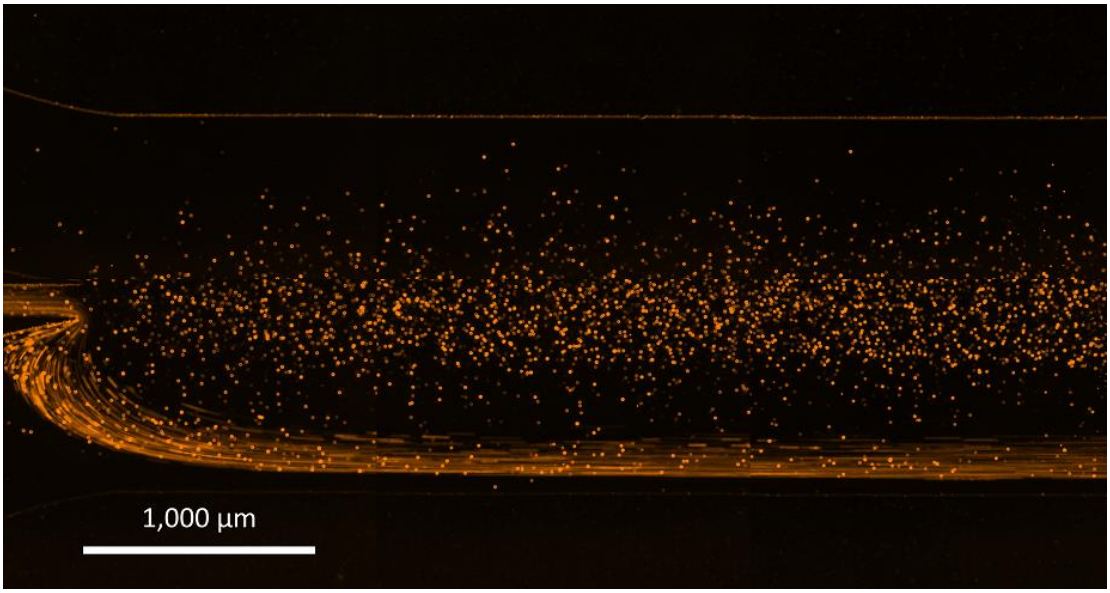

Figure 4-5. Flow fluctuations causing the cell solution to flow back into one of the feeder channels, thus obscuring any chemotactic response. Due to flow rate and exposure time, moving cells are observed as lines tracking their path, while cells that do not display a linear path are non-motile and have adhered to the PDMS channel walls.

This effect can be mitigated through the use of more consistent pumps, introducing the solutions at higher flow rates, or altering the device design or dimensions. However, the former solution can be prohibitively expensive for many lab groups, while the latter two solutions introduce other sources of error or suppress bacterial chemotaxis, for reasons discussed in other sections of this thesis.

4.3 Non-Linear Gradient Shape

An additional concern is the overall gradient shape. The micromixers split the solutions into six channels, which rejoin into two channels which then feed into the main channel. However, some diffusion occurs while the solutions travel through the two channels before joining the main channel, leading to a concentration gradient across the channel width that follows a Boltzmann distribution. While this is preventable by having all micromixer channels join at the main channel, in practice this is difficult to operate due to the increased complexity at the channel entrance trapping bubbles more frequently, even more difficulty in controlling flow fluctuations as discussed in the previous section, and additional design concerns relating to the seventh channel needed for introduction of the cells. Fig. 4-6 shows a comparison of the gradient at the channel beginning in the two-channel and the six-channel format (note that neither device design was simulated with the inclusion of the cell inlet, for the sake of simplicity).

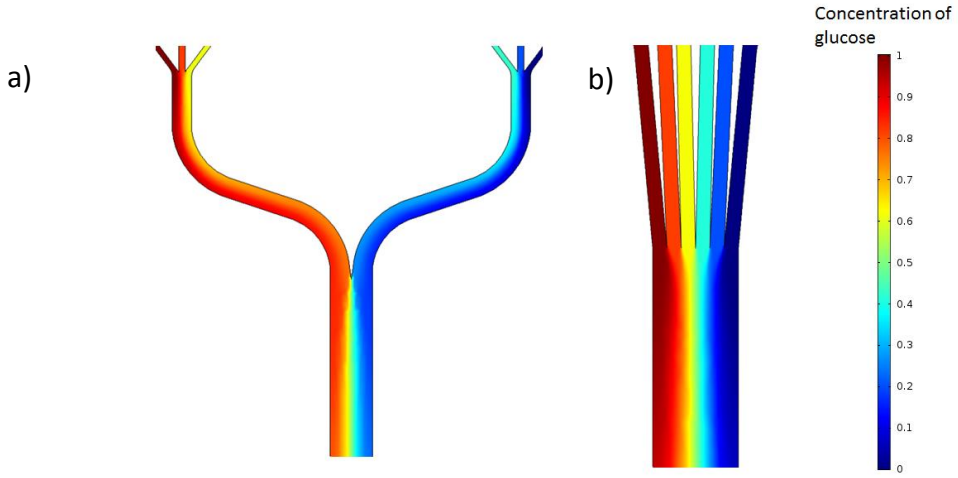

Figure 4-6. Comparison of the concentration distribution of glucose, at a flow rate of 1.0 μL/min through each inlet. a) Device design where the 6 channels from the micromixer array are first merged into two feeder channels before forming the main channel. b) device design where the 6 channels from the micromixer array remain separated until joining to form the main channel.

Chemotaxis is best observed in a linear gradient, so that any changes in chemotactic behavior are not a function of gradient shape and can instead be traced to other factors under examination. Furthermore, the flattening of the gradient near the channel sidewalls can prevent visible chemotaxis, since in a constant concentration of a chemoattractant, a bacterium will experience extended run lengths but no directional bias.

The gradient was also visualized experimentally, by generating a gradient of fluorescein in deionized water from 0 mM to 1 mM. The gradient was generated with flow rates of 1 µL/min through each inlet (2 µL/min total) and 0.1 µL/min through each inlet (0.2 µL/min total). Fig. 4-7 shows the resulting gradients and the corresponding ImageJ analysis of the fluorescence intensity across the main channel width, at the beginning and end of the channel.

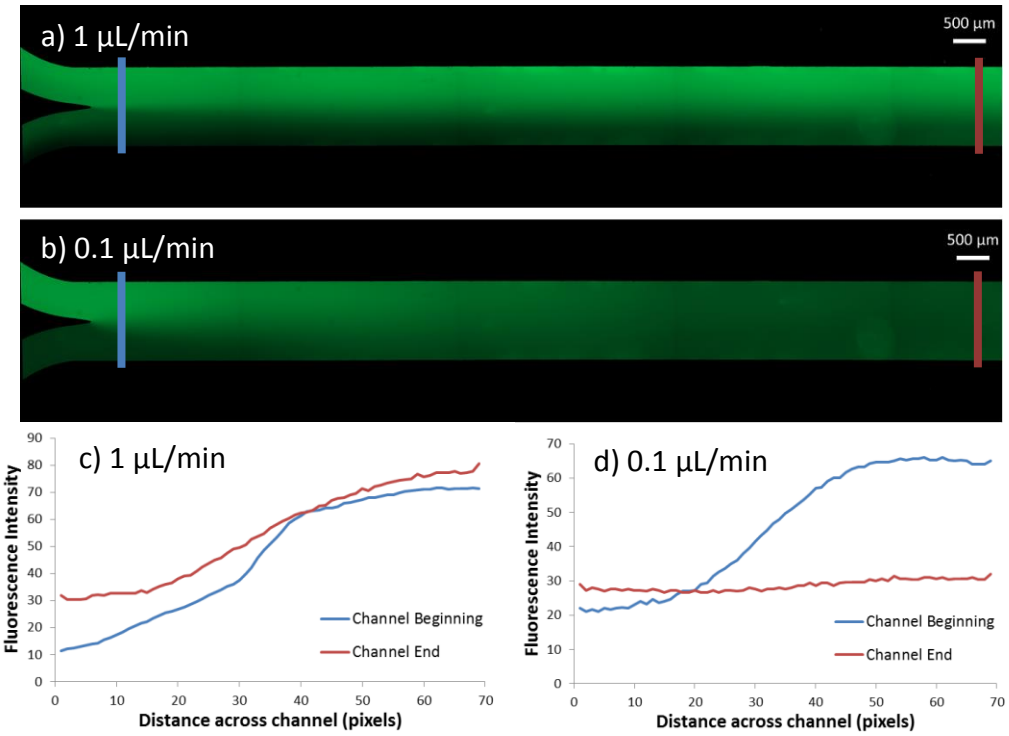

Figure 4-7. Images of the gradient formed in this device at flow rates of a) 1 µL/min, and b) 0.1 µL/min, and analysis of the fluorescence intensities across the channel width at the cut lines shown for c) 1 µL/min, and d) 0.1 µL/min.

This closely corresponds to the results obtained with COMSOL simulations. The higher flow rate maintains a gradient down the channel length, although diffusion does lead to gradient flattening. At the lower flow rate, the gradient quickly flattens, and appears to be completely flat by the time it reaches the end of the channel. While the fluorescence intensities were not normalized, the shape of the gradient is what demonstrates the gradient decay, since variations in ambient light can affect the analyzed intensities.

4.4 Local Gradient at Cell Inlet

The cell solution presents an additional complication for the rapid formation of linear gradients. The cells are suspended in a solution that does not contain any chemoeffector, so that at the center of the main channel there is a discontinuity in the gradient. As diffusion continues down the channel length, the cells experience a small local gradient initially, as shown in Fig. 4-8.

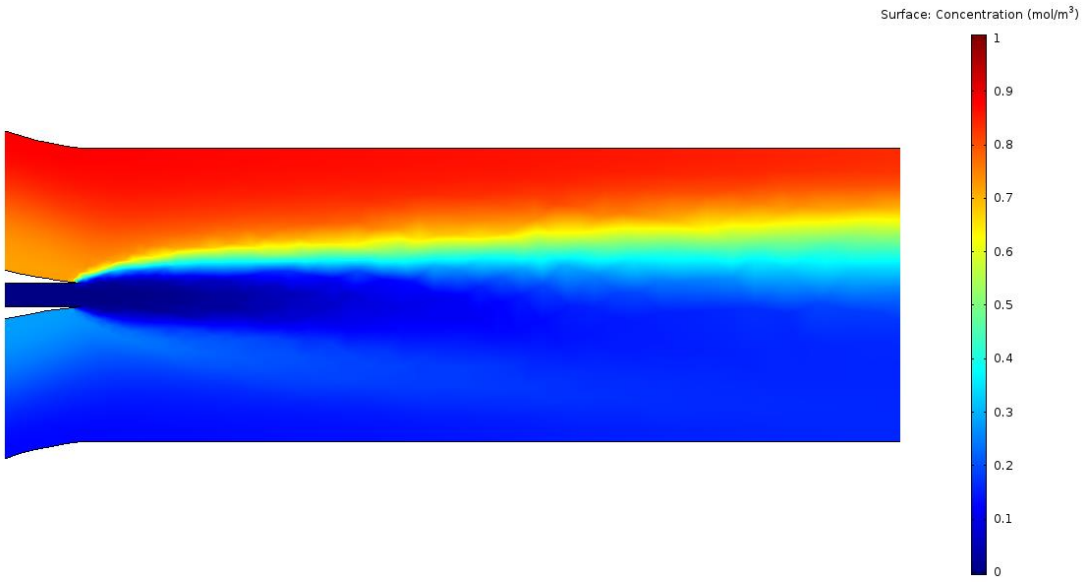

Figure 4-8. COMSOL multiphysics simulation of the gradient disruption created by the cell inlet, where the chemoeffector simulated is glucose, and the flow rate is 1 μL/min through each of the two upstream inlets and 0.17 μL/min through the cell inlet.

This can cause the initial chemotaxis of the cells to be relatively equivalent towards both directions, and a chemotactic response that is more reflective of the overall concentration gradient cannot be observed until further down the channel. Fig. 4-9 shows the concentration across the channel width at the point where the cells are first introduced, and at a point 2300 microns down the channel length, which is the approximate point at which this effect is no longer apparent and there is no longer a dip in the concentration.

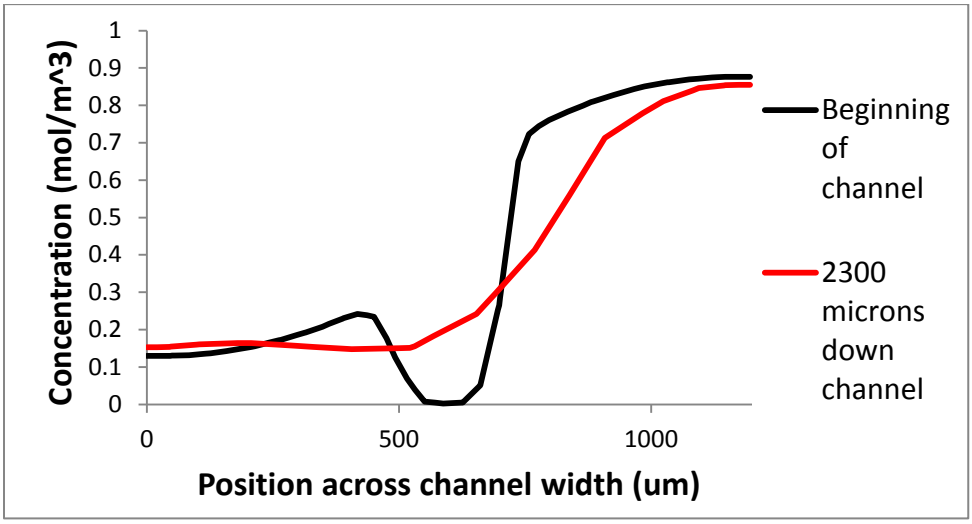

Figure 4-9. Plot of the concentration gradients resulting from the cell inlet disruption depicted in Fig. 4-8. A cut line across the channel width was taken immediately where the cell inlet joins the main channel, and 2300 microns down the channel length, just prior to where the "dip" in the concentration gradient disappears.

4.5 Optimizing Concentration

Chemotactic bacteria are very sensitive to concentrations of a chemoattractant, and their chemotactic response can be maximized at certain concentrations, as demonstrated by Mesibov and Adler in 1972 and Adler, et al. in 1973[12,13]. However, this determination was performed using the capillary assay described earlier, where the concentration of the chemoattractant solutions in the capillary were altered and

the concentration yielding the maximum response was reported as the concentration at which the most bacteria accumulated in the capillary. In practice, this may not translate well to a microfluidic device. For example, the chemoattractant concentration which yielded the maximum response may have actually occurred near the capillary tip, where the chemoattractant was diluted to a much lower concentration. As a result, if this concentration of chemoeffector solution were utilized in a microfluidic device, the chemotaxis response might not be maximized, and any chemotaxis would be unnoticeable. A range of concentrations would need to be tested to determine the optimal concentration in a microfluidic device, but this is a time-consuming process and requires more resources than testing with a capillary assay or an agar plate assay. Additionally, even if concentrations were tested in a microfluidic design, in the case of little to no response it may be difficult to decipher whether it was an effect of the concentration range or the other many sources of error present in these devices.

4.6 Bacterial Adhesion

A general issue with the observation of bacteria in microfluidic devices is the solution in which the bacteria are dispersed. Bacterial behavior is attenuated by the media or buffer in its environment. Originally, the bacteria were exposed to an environment that was primarily PBS. The bacteria solution was in D-PBS, which contains calcium and magnesium, but the buffer and chemoeffector solution introduced into the microfluidic gradient generators comprised the majority of the solution in the channel. Through diffusion of the chemical species and the bacteria themselves, the bacteria's microenvironment rapidly changes, and the concentration

of calcium and magnesium drops off significantly. In response, a large fraction of the bacteria became immobilized on the PDMS surfaces, as shown in Fig. 4-10, where streaks or lines are cells that are not adsorbed on the PDMS walls, and single points are cells that are adsorbed. In this image, a fluctuation in flow as described in 4.2 has made the cells that have adsorbed on the PDMS surface visible, as they are no longer convoluted by the flowing cells.

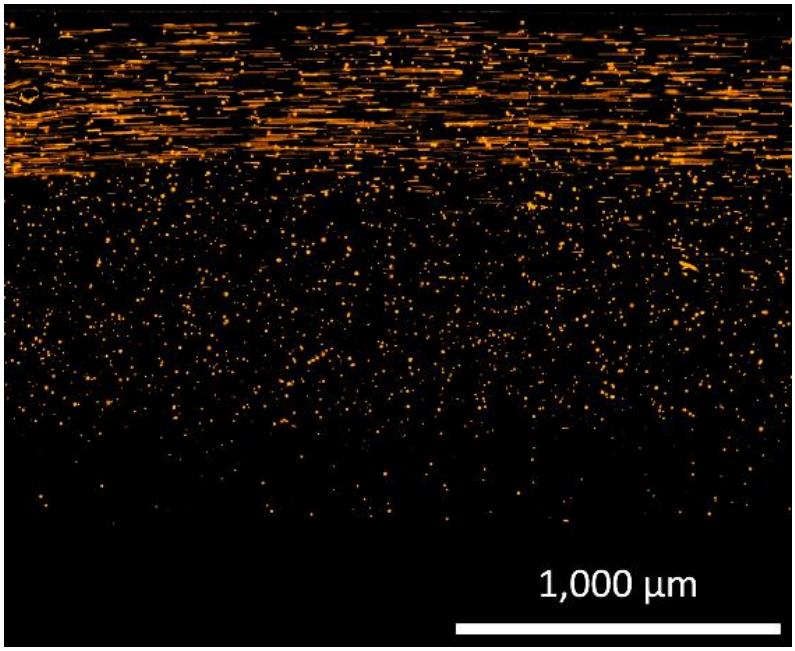

Figure 4-10. Bacteria adsorbed on the PDMS surfaces of the main channel. Flow fluctuations as described in 4.2 lead to cells flowing to the side. Cells that are not adsorbed are visible as streaks or lines, whereas cells that are adsorbed are visible as single points.

Adsorbed bacteria on the PDMS surface obscure the movement of free-swimming bacteria, and as the density of adsorbed bacteria increases with increased experiment length, it becomes increasingly difficult to observe any chemotaxis that may be occurring. Two methods for preventing this response were characterized. Initially, bacterial adhesion to PDMS was then tested in solutions of D-PBS and LB media. *E. coli* with O.D. 0.6 were prepared in D-PBS. 400 µL of the bacterial solution

were then combined with 600 μL of PBS, D-PBS, PBS with 5% LB media, or PBS with 10% LB media. This solution was introduced to a microchannel of dimensions 50 μm height and 200 μm width. The devices were allowed to sit for 10 minutes, then rinsed with PBS at a rate of 250 μL/minute for two minutes, and the resulting cell adhesion was observed after flow was stopped. Fig. 4-11 shows the results of these tests.

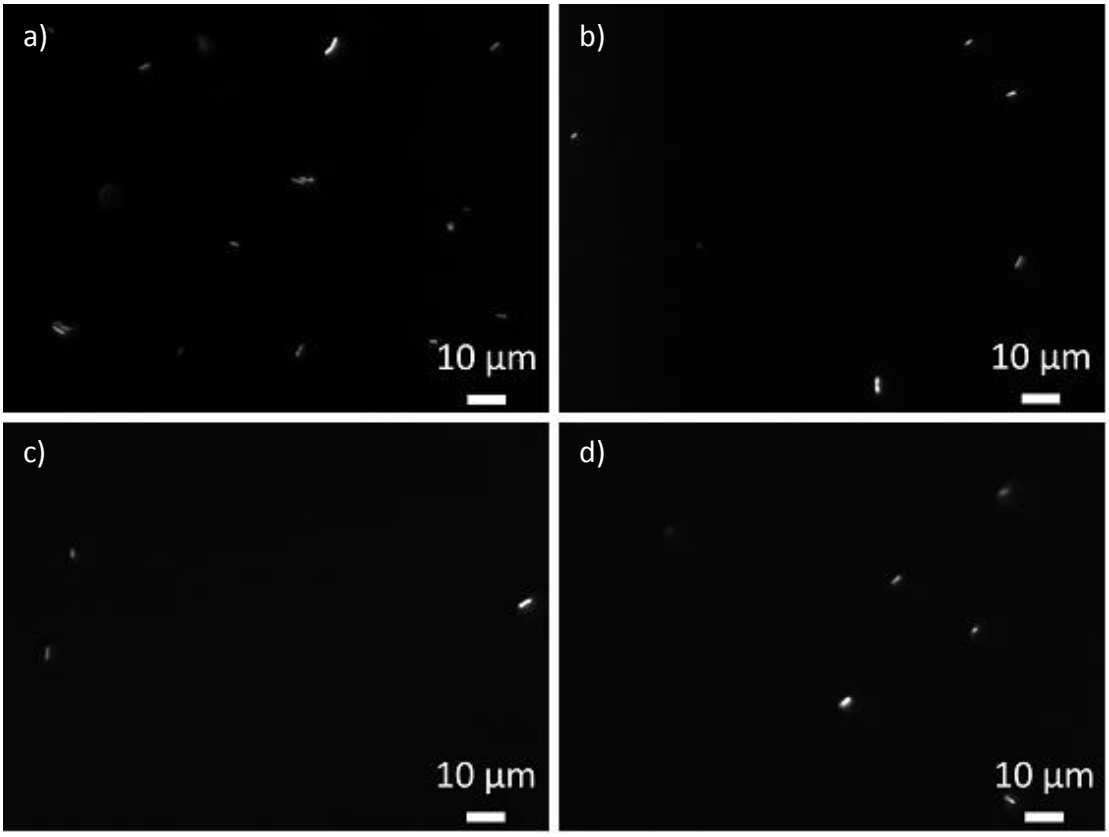

Figure 4-11. Images of cell adhesion tests, where cells are dispersed in solutions of a) PBS only, b) D-PBS only, c) PBS with 5% LB media, or d) PBS with 10% LB media.

The average number of cells per square micron adsorbed on the surface of the microchannel was 1.17×10^{-3}, 4.14×10^{-4}, 2.07×10^{-4}, and 3.45×10^{-4}, for PBS, D-PBS, 5% LB media, and 10% LB media respectively. The cells in 10% LB media exhibited more adhesion than the cells in 5% LB media, which may be due to

not examining enough frames to obtain a large set of data, or may indicate that the benefits of adding LB media to the cell solution level off after reaching approximately 5%.

An alternative solution that does not require changing the bacteria solution utilizes bovine serum albumin to treat the surface of the PDMS. Microfluidic devices were filled with 2 mg/mL BSA, left at room temperature for 10 minutes, and then gently rinsed with 1 mL of PBS. BSA is a protein that is commonly used as a blocking agent, since it is hydrophilic when folded, but is able to form a layer on PDMS and is biocompatible[35]. While adhesion tests similar to those shown in Fig. 4-11 were not performed for BSA pretreated channels, videos taken of cells flowing in these channels demonstrate that adhesion is significantly reduced through this method.

Chapter 5: Theoretical Analysis

A significant number of experimental factors can make it difficult to achieve observable bacteria chemotaxis in a flow-based microfluidic gradient generator, as described in the previous chapter. However, it is important to also examine these devices from a theoretical perspective, to determine if the principles behind them support the conclusion that they can be used for this application. This chapter will examine several fundamental properties of these devices: the balance of gradient decay and residence time, the effects of fluid shear in Poiseulle flow, the distribution of bacteria in a microchannel geometry, and the effect of a decaying gradient. Additionally, a simplified method for calculating the concentration in a microchannel is developed for applications in future simulations.

5.1 Gradient Decay and Residence Time

These devices offer a distinct advantage in the creation of highly controlled gradients; however, they also possess some flaws that can affect results for chemotaxis experiments. One of the most significant flaws is something that has also been touted as an advantage of these systems—their ability to generate stable gradients. Since they are flow-based, the chemical gradient will remain the same at any time point, limited only by the amount of solutions available to inject into the device. However, the individual bacteria are not exposed to a stable gradient—once introduced to the main channel, they flow at the same rate as all the solutions in the channel and the gradient they experience will decay in the same manner as if the flow were stopped entirely and the resulting temporal decay observed within the channel.

Additionally, there is a tradeoff between gradient decay and residence time in the channel. As the solution moves down the channel, more diffusion occurs and the gradient becomes less steep, which can eventually lead to a flat concentration profile across the channel width. At high flow rates this will not occur, but increasing the flow rate reduces the amount of time bacteria spend in the channel, and the bacteria will need a suitable amount of time to sense the gradient and swim far enough towards or away the chemoeffector to make the pattern visually apparent. A simulation of the gradient for 1 mM glucose is shown in Fig. 5-1 for total flow rates of 0.2 and 2.0 μL/min (0.1 and 1.0 μL/min per each inlet). The dimensions of the main channel are 18,000 μm long by 1,200 μm wide by 50 μm high, so these flow rates correspond to residence times of 324 and 32.4 seconds, respectively.

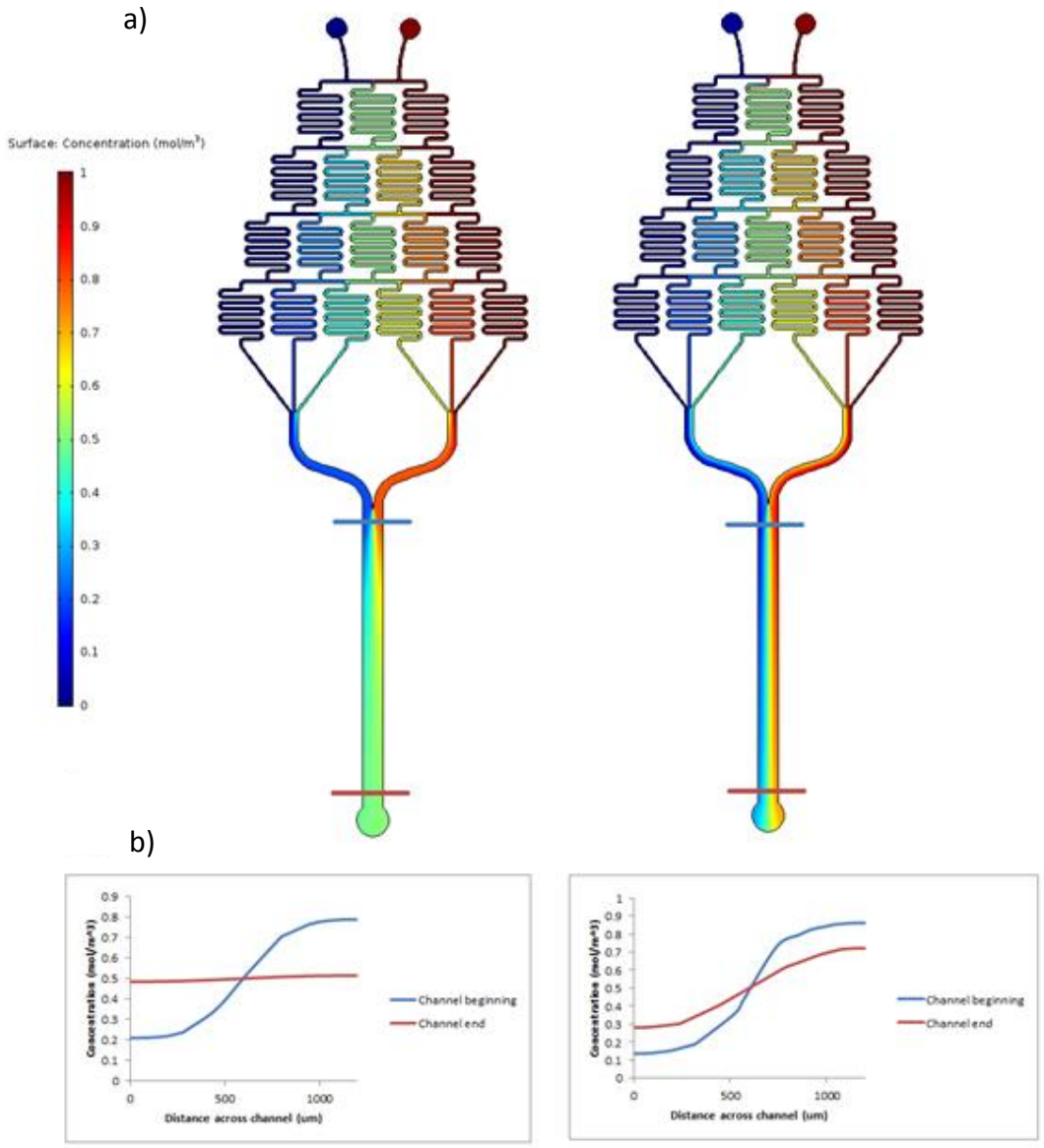

Figure 5-1. a) COMSOL Multiphysics simulations of the concentration of glucose at flow rates of 0.1 µL/min and 1 µL/min. b) Corresponding cross-sectional concentration profiles taken at the beginning and end of the main channel, as indicated by the cut lines in (a).

E. coli bacteria have a maximum swimming speed of approximately 25 microns per second[36]. Thus, for the above residence times, the bacteria would be able to move a maximum distance of 8100 microns and 810 microns, respectively. While this distance could correspond to visible chemotaxis, this would require that the

bacteria swim at this speed continuously, do not experience any tumbling events, and swim in a relatively linear path towards the channel sides. This is very unlikely given the "run-and-tumble" pattern of bacterial movement and the attenuating effects of shear flow.

Additionally, Vladimirov et al. demonstrated the speed of a bacterium in a concentration gradient depends linearly on the steepness of the concentration gradient, and found that in practice the speed of a bacterium in a very steep gradient was unlikely to exceed 15 microns per second[37]. A steep gradient is only maintained for several seconds in the main channel before diffusion causes it to decay and suppress observed chemotaxis. Design modifications cannot delay gradient decay; changing the channel dimensions with respect to a constant volumetric flow rate will result in changes in the flow velocity. Increasing the channel volume will decrease the flow velocity and lead to greater gradient decay, while decreasing the channel volume will increase flow velocity and lower the residence time. Fig. 5-2 plots the drop in concentration across the channel width near the outlet as a function of the residence time to demonstrate this. Changing the geometry of the channel will optimize one of these variables at the expense of the other.

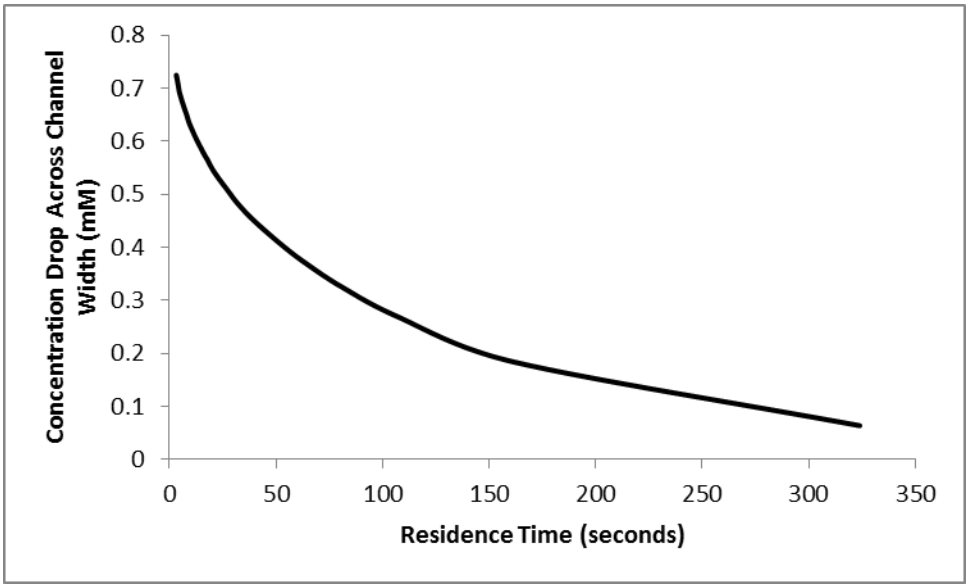

Figure 5-2. A plot of the residence time in the main channel for a single bacterium versus the concentration drop across the channel width that occurs by the end of the main channel. A flow rate of 1μL/min through each individual inlet would correspond to a residence time of 32.4 seconds,, and a flow rate of 0.1 μL/min through each outlet would correspond to a residence time of 324 seconds.

5.1.1 Cell Population Simulations

Vladimirov, et al. designed a Javascript program capable of simulating the distribution of bacteria in a gradient of aspartate over time[37]. While this model only demonstrates simulated outcomes in a static environment with a stable gradient, it can be used to approximate the upper limits of an observable chemotactic response. Additionally, the response to aspartate can be considered as representative of chemotaxis in general. It is normally used as a "model" chemoattractant because it generates a clear and rapid chemotactic response, and other chemoattractants will either generate a similar or less pronounced response, again indicating that the results obtained with this program can be considered the "upper limit" of chemotactic response that could be obtained with the defined experimental conditions.

This model uses a hybrid approach to simulation, where receptor activity is modeled via mean-field approximation, the methylation state of the receptors is modeled by ordinary differential equations, the phosphorylation of the Che transduction pathway is modeled algebraically, and the flagellar motors are modeled as stochastic switches[38]. Other values, such as the binding constant of the Tar receptor to aspartate, the concentrations of [CheB] and [CheR] within a cell, and the counterclockwise motor bias of the flagella are predetermined. The swimming speed during a run is assumed to be constant at 20 μm/sec. The result is a computationally light program capable of simulating large populations of bacteria over long time periods, with results that correspond to experimental fluorescence resonance energy transfer data[39].

In this program, the area is defined as a 1 mm x 1 mm square, where the concentration of aspartate is 0 mm at the left wall and linearly increases to 1 mm at the right wall. It should be noted that 1 mm is a commonly used width for microfluidic gradient generators, and corresponds to that used by Englert et al. in their device, off of which the device in this thesis is based[33]. The bacteria are all initially located at the exact center of the defined area. A linear gradient is defined from 0 mM aspartate at the left wall to 1 mM aspartate at the right wall. Fig. 5-3 shows the predicted distribution of a population of 200 bacteria after times of 25 seconds, 50 seconds, 100 seconds, 200 seconds, 300 seconds, and 400 seconds (after which there were no discernible changes in the bacteria distribution). The area is shaded to approximate the concentration gradient of aspartate.

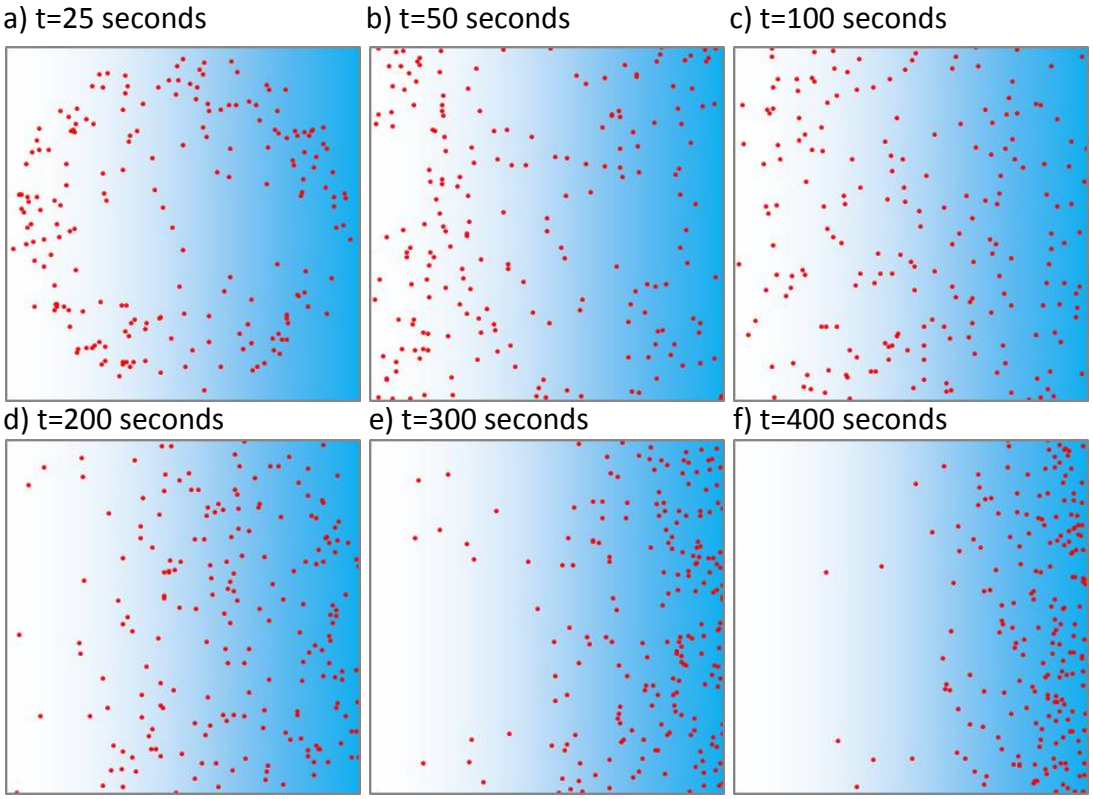

Figure 5-3. The distribution of a population of 200 E. coli cells in a linear gradient of aspartate from 0 mM on the left to 1 mM on the right, at a) 25 seconds, b) 50 seconds, c) 100 seconds, d) 200 seconds, e) 300 seconds, and f) 400 seconds. Little visible change was observed after 400 seconds.

Englert, et al. indicate that the residence time of a bacterium in the main channel of their device is approximately 18-21 seconds[33]. However, the "best-case scenario" results obtained with this program indicate that after this time no chemotaxis is discernible, and the bacteria are just beginning to disperse from the cell inlet at the center of the channel. Effects detailed later in this chapter, such as shear and bacteria trapping near microchannel walls, will further attenuate any bacterial movement, thus implying that this time frame is not nearly long enough for successful demonstration of chemotaxis.

5.1.2 Experimental Results for PDMS Interactions

Englert, et al. claim that bacteria flagella colliding with microchannel walls in a device slows the total residence time in a channel to approximately three times what it would be without this effect[33]. As in earlier tests, some cells permanently adhered to the PDMS surfaces, whereas others remained free-swimming. During tests with a 50 micron high device, several bacteria were tracked across the camera field of view during a video, and their speed was calculated. Fig. 5-4 shows an example of a bacterium that was tracked at its starting and ending positions.

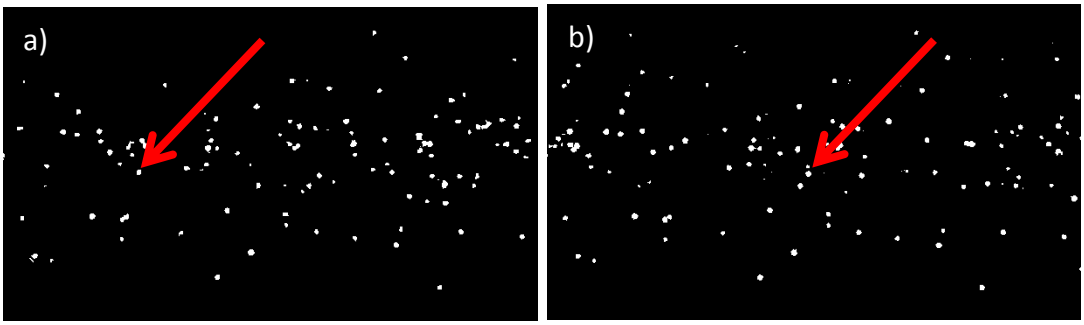

Figure 5-4. Images of bacteria flowing in the main channel at a rate of 0.1 μL/min through each of the three inlets. a) Initial positions of an example bacterium. b) Position of the bacterium after 10 seconds.

For flow rates of 0.1 μL/min through each of the three inlets, this corresponds to a displacement rate of 5,000,000 μm^3/second. Thus, the average speed along the channel in the x-direction is approximately 83 μm/second. The results obtained experimentally are shown in Table 5-1.

Table 5-1: Experimental data for displacement along the channel length and time period of displacement taken from videos of bacteria flowing in a channel, and the resulting calculation of the speed at which the bacteria are flowing.

X Displacement (microns)	Time (seconds)	Speed in X Direction (microns/second)
1040	14	74
780	10	78
820	12	68
1240	16	78
480	7	69

While these results are preliminary and further data utilizing more sophisticated tracking is required to confirm them, they may indicate that the residence time of a bacterium in the main channel is not substantially increased by flagella interactions with the channel walls. However, even if this phenomenon did occur, this would not necessarily be useful for chemotaxis characterization. If the interaction of a bacterium's flagella with the side wall was significant enough to increase its residence time to three times what it would be otherwise, then this interaction is almost certainly significant enough to alter the motility and path of the bacterium's chemotaxis. This would most likely obscure or attenuate any observed chemotaxis in the main channel, indicating that these interactions are not a desirable solution for extending the residence time of the bacteria in the main channel.

5.2 Fluid Shear

However, the most significant factor that prevents flow-based microfluidic chemotaxis platforms from realizing clear results is the presence of shear flow. Shear

flow can suppress lateral movement, especially in the case of bacteria with low motility, and may indicate a lack of chemotactic function when this is not the case.

E. coli bodies are ellipsoidal, and in a microchannel experiencing Poiseulle flow, the varying rates of shear across the channel width produce a torque on an individual bacterium. The simulated shear across the channel width is shown in Fig. 5-5 for flow rates of 1 μL/min and 0.1 μL/min per each individual inlet, which corresponds to 2 μL/min and 0.2 μL/min total through the device, respectively.

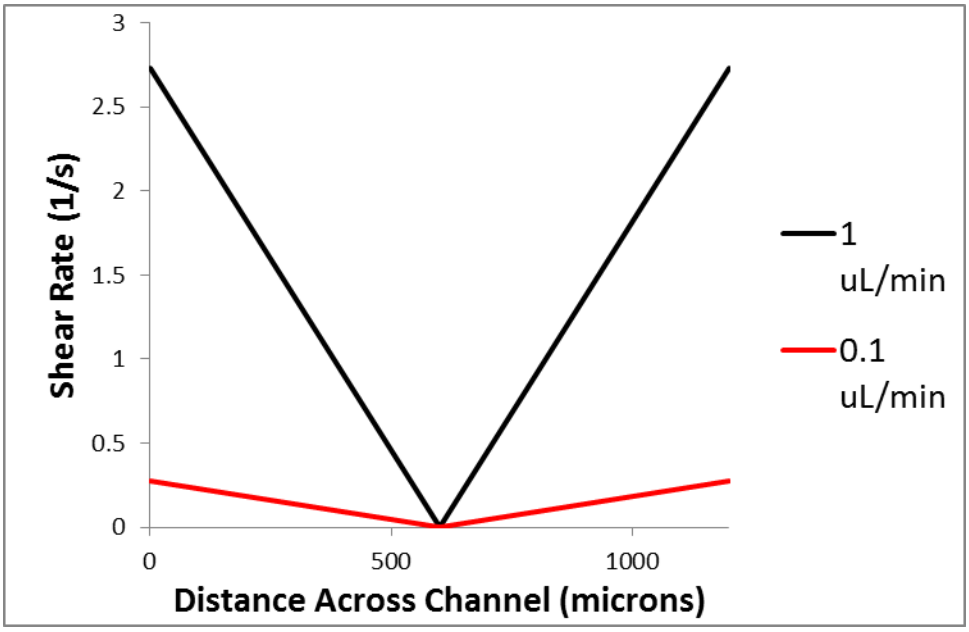

Figure 5-5. Visualization of shear across the main channel width of the microfluidic gradient generator for two flow rates.

The result is that the bacterium is continually reoriented by this external force, and thus is less able to accurately determine the appropriate directional bias to reach an area of higher concentration of a chemoattractant. In a static environment, bacteria have persistence of direction, such that their swimming trajectories before and after tumbling events are correlated. Bearon and Pedley have developed a model for movement of a prolate spheroid in a flowing environment, and Locsei and Pedley

further built upon this model[40,41]. Fig. 5-6 shows their results for the normalized drift velocity, which is the mean velocity up the chemoattractant gradient, as a function of a shear strength parameter. The different curves correspond to different slenderness ratios.

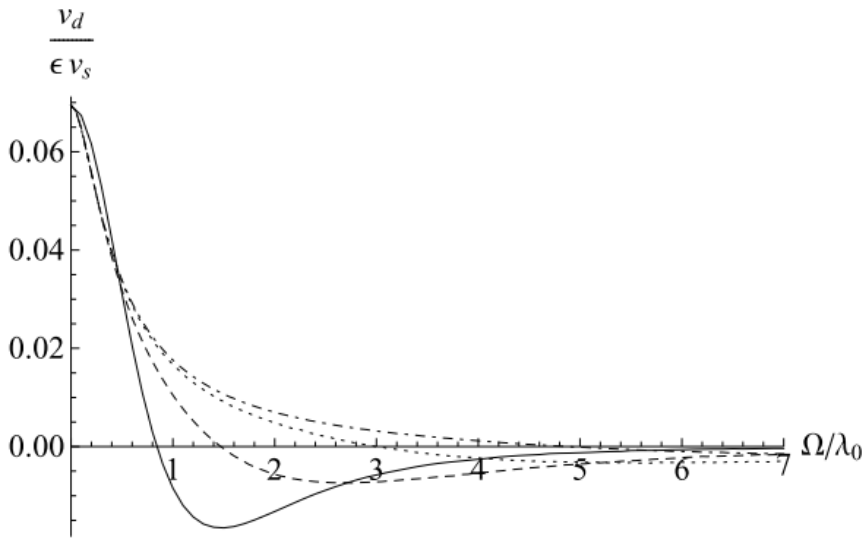

Figure 5-6. Chemotactic drift velocity, divided by a normalizing factor, as a function of the shear parameter. The shear parameter is the shear rate, divided by two, and for this plot the shear parameter is then divided by the baseline tumble rate of the bacterium (typically1 per second). The different curves correspond to different slenderness ratios (the ratio of the major to minor axis), where the solid line is for slenderness ratio=1 (a sphere), the dashed line is for slenderness ratio=4, the dotted line is for slenderness ratio=9 (approximated as fitting *E. coli*), and the dot-dashed line is for slenderness ratio=15. Reprinted with permission from *Bulletin of Mathematical Biology*, 2009, **71**(5), 1089-1116[41].

Significantly, Pedley and Locsei found that above shear rates of 2 s^{-1} ellipsoidal bacteria display negative chemotaxis, meaning the bacteria are moving down a chemoattractant gradient, and that even below this threshold the chemotactic response is severely attenuated.

Additionally, Tournus, et al. performed simulations to demonstrate the complex trajectories a bacterium follows in shear flow, and incorporated the effects of flagella into their work[42].

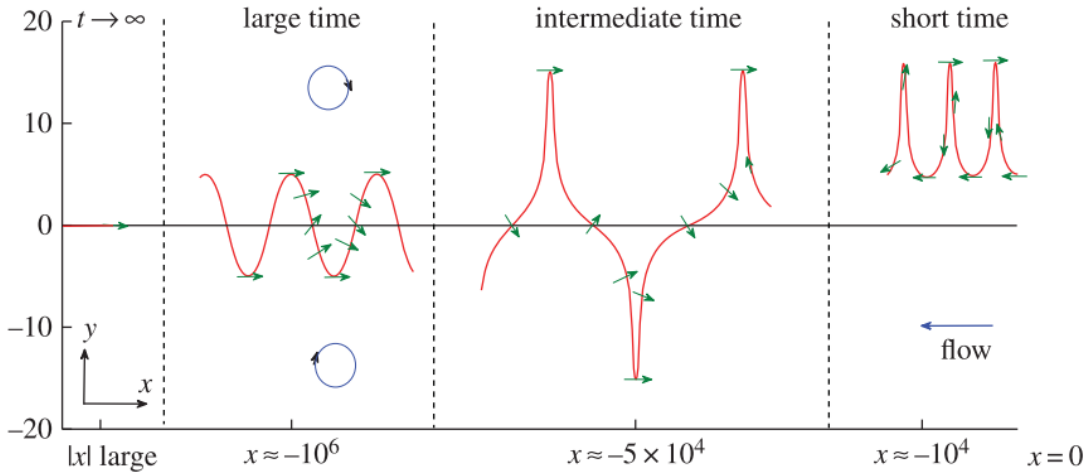

Figure 5-7. The trajectories of a bacterium in shear flow at different times after release. The green arrows correspond to the bacterium's orientation, and the blue arrows depict the vorticity. The bacterium's trajectory initially follows loops in one half of the channel, then spreads to form loops in both channels at intermediate times. The amplitude of the loops gradually decreases, and eventually the bacterium travels in a straight line down the center of the channel, with orientation against the flow. Reprinted with permission from *Proceedings of the Royal Society of London A*, 2014, **12**(102), 1-11[42].

5.3 Bacteria Population Distribution

The varying flow velocities and shear rates across the channel width also lead to different distributions of a bacterial population, as compared to a flow-free environment. Molaei, et al. demonstrated that bacteria accumulate near the channel walls, and Rusconi, et al. also showed that they are depleted from the center of the channel, thus obscuring the chemotactic effect[43,44].

The nature of laminar flow will create a different velocity profile across the width of the channel, where the velocity is highest at the center of the channel, and lowest near the walls. This can lead to a depletion effect, in which swimming bacteria become trapped near the side walls of the microchannel and the concentration of cells near the center of the channel (where chemotaxis would occur most rapidly due to the steepness of the gradient) drops significantly. Figure 5-8 shows results obtained by

Rusconi, et al. that demonstrate the significance of this effect in microchannels, and proved that it is dependent on cell swimming, since dead cells are not similarly depleted.

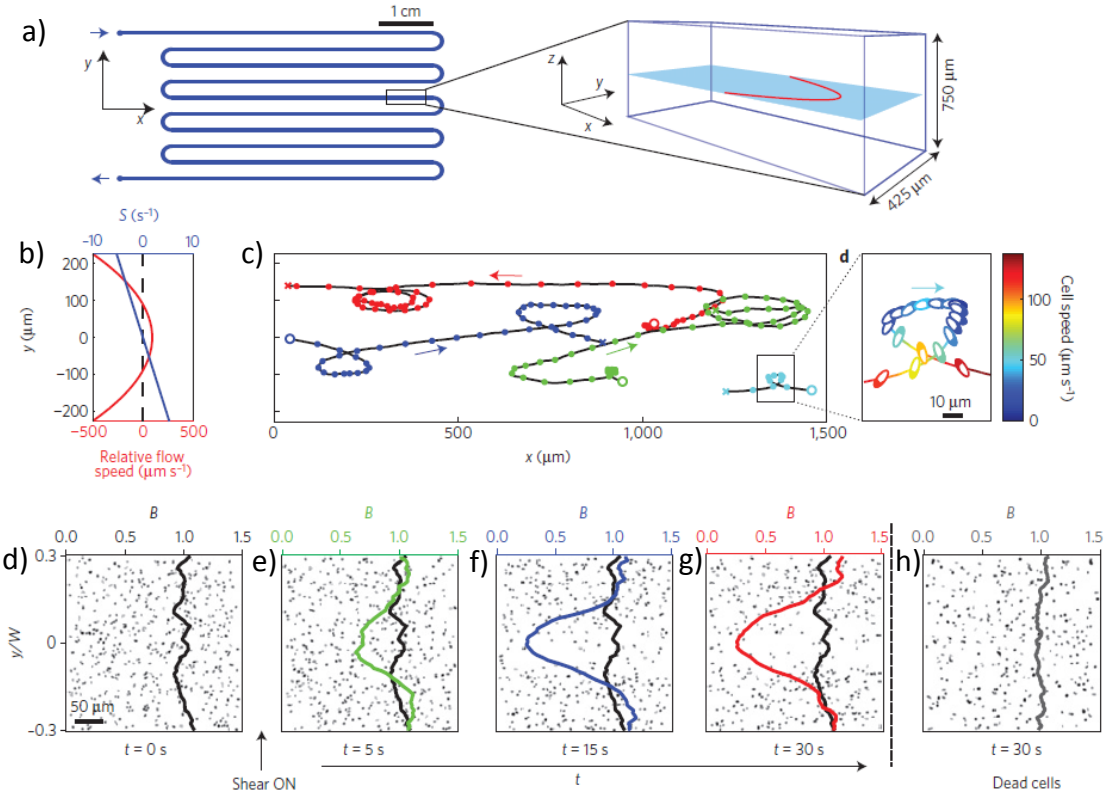

Figure 5-8. a) Schematic of the serpentine channel design used, and an inset showing the parabolic flow rate through the channel. b) Plot of the parabolic flow rate and the shear rate across the channel width. c) Trajectories of *Bacillus subtilis* bacteria tracked in the microchannel, and an inset showing the trajectory, orientation, and speed of a single bacterium. d-g) Phase-contrast images demonstrating the evolution of the distribution of *B. subtilis* cells in a microchannel, where the colored lines correspond to the current distribution of cells at that time point, while the black line indicates the initial distribution. h) Distribution of dead *B. subtilis* cells in the same flow conditions, showing no depletion. Reprinted with permission from *Nature Physics*, 2014, **10**(3), 212-217[43].

5.4 Deteriorating Gradient Effect

This also ignores the effects of a decaying gradient on chemotactic behavior. Due to gradient decay, even if an individual cell swims towards the channel side with a higher chemoattractant concentration, it may experience a lower local concentration

during its next tumbling event, causing run length to shorten and tumbling frequency to increase. This is shown in Fig. 5-5 by a COMSOL simulation of the concentration profiles at the beginning of the main channel for flow rates of 1 µL/min and 0.1 µL/min, and a plot of the concentration as a function of position down the channel length at 1000 microns across the channel width for a flow rate of 0.1 µL/min.

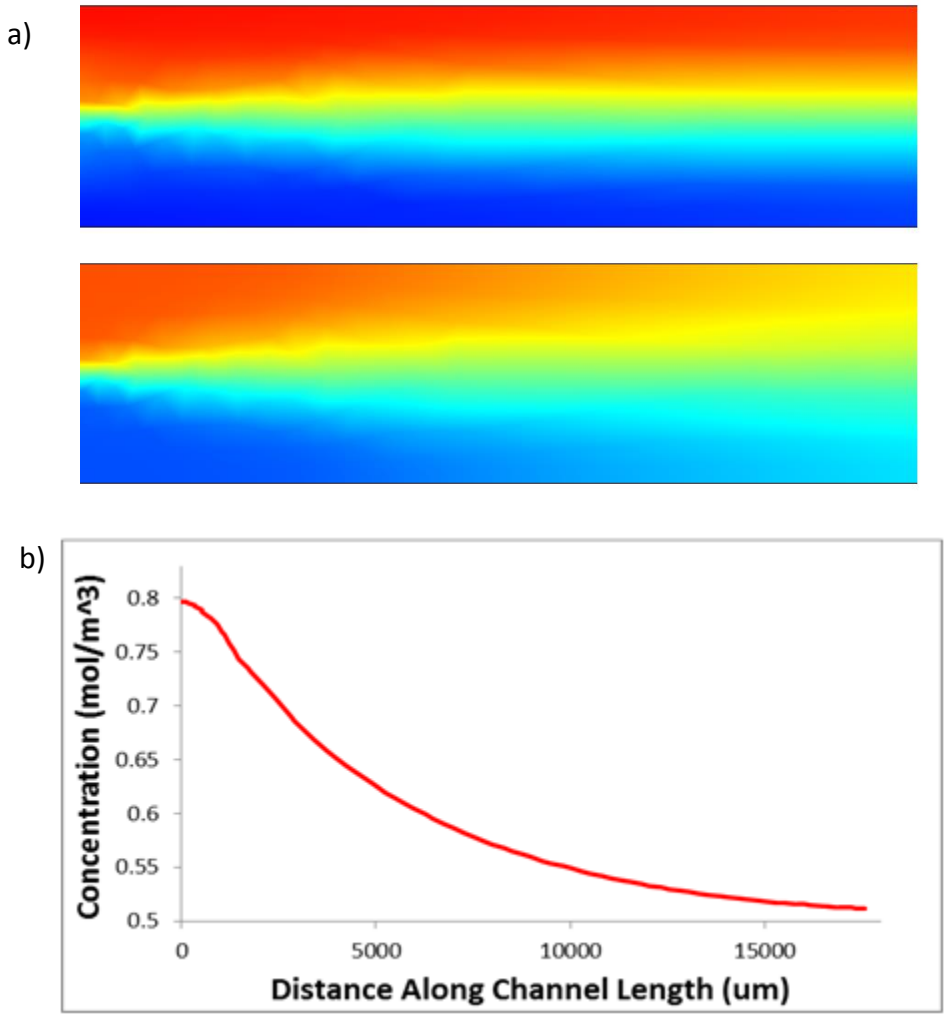

Figure 5-9. a) Concentration gradient decay along the channel length for flow rates of 1 µL/min and 0.1 µL/min through each individual outlet. b) The concentration drop along the channel length at 1000 microns across the channel, or 200 microns away from the wall with the highest concentration of chemoattractant.

When the bacterium travels in a line parallel to the channel axis or relatively close to this movement path, it cannot outrun the diffusion. Since a single *E. coli* bacterium is approximately 0.5 μm wide and 2 μm wide, it will diffuse at a significantly slower rate than the chemoattractant molecules. This is especially important during tumbling events, which last on average 0.1 seconds. Since a bacterium is not swimming during a tumble, its position is governed by the flow of solution in the microchannel and diffusion. Thus, after it completes the tumbling event its immediate environment will have a lower concentration. For a tumbling event of 0.1 seconds, at the location across the channel width from the graph above, this could correspond to a concentration drop as high as 0.15 millimolar, which is substantial when experienced by a bacterium that is sensitive to changes in its external environment. This results in a decrease in the bacterium's average swimming speed, and thus it is increasingly unable to outrun the diffusion of the chemoattractant.

5.5 Simplified Method for Concentration Calculations

A simplified method of determining the concentration gradient in a microfluidic gradient generator is useful for precise simulations of chemotactic behavior. This is accomplished using COMSOL simulations as a starting point. Here, the concentration profiles at the beginning and end of the main channel, shown earlier in Fig. 5-1 for different flow rates, can provide this information. Equations for these profiles can be approximated using a Boltzmann curve fit, obtained with OriginLab. Plots of these curve fittings are shown in Fig. 5-6, and the corresponding equations for the fitted curves are given in Appendix A.

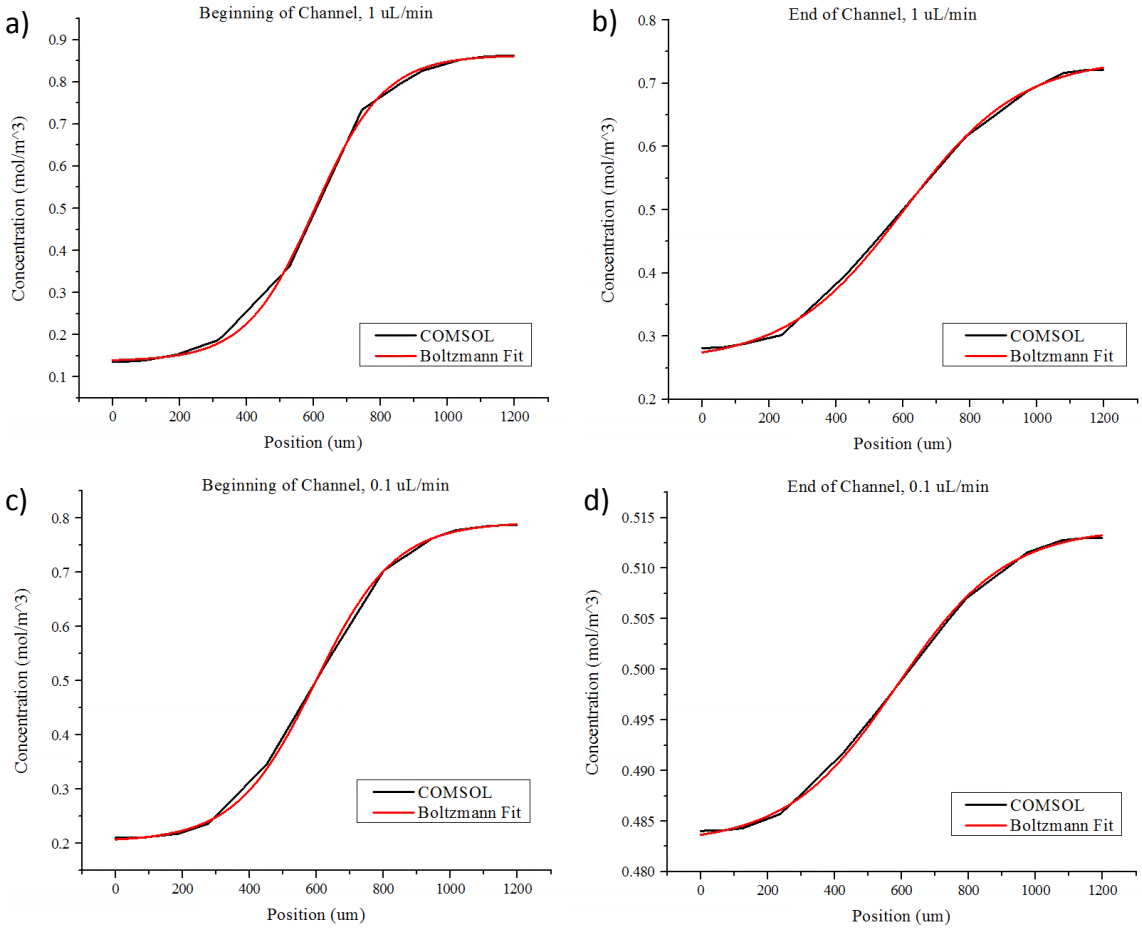

Figure 5-10. Plots of the concentration gradients across the channel width obtained using COMSOL multiphysics, and the Boltzmann curve fitting equations obtained with OriginLab, for a) the beginning of the channel at 1 µL/min, b) the end of the channel at 1 µL/min, c) the beginning of the channel at 0.1 µL/min, and d) the end of the channel at 0.1 µL/min.

The x-values are normalized by the channel width, so that any width value can be substituted for W to adjust these distributions, and shifted so that the center of the channel corresponds to x=0. Using the equations in Appendix A, two sets of coordinates can be found as a function of the bacterium position across the channel width, where the y-values correspond to the concentration and the x-values correspond to the position along the channel length. These coordinates can be substituted into an exponential equation of the form:

$$y = Ae^{x/B} + C$$

Once the constants A and B are determined (C is 0.5 due to the geometry of the device), the distance along the channel length can be substituted for x and the exact concentration determined. This equation follows the form:

$$y = (y_1 - 0.5)e^{\left[x \Big/ \frac{x_2}{ln\left(\frac{y_2-0.5}{y_1-0.5}\right)}\right]} + 0.5$$

where x_2 is the distance down the channel length of the second cut line (in this case, 17700 microns), y_1 is the concentration at the first cut line at the specified distance across the channel width, and y_2 is the concentration at the second cut line at that distance. A comparison of the results from COMSOL and the results from this simplified method along the channel length at 1000 microns across the channel width is shown in Fig. 5-7.

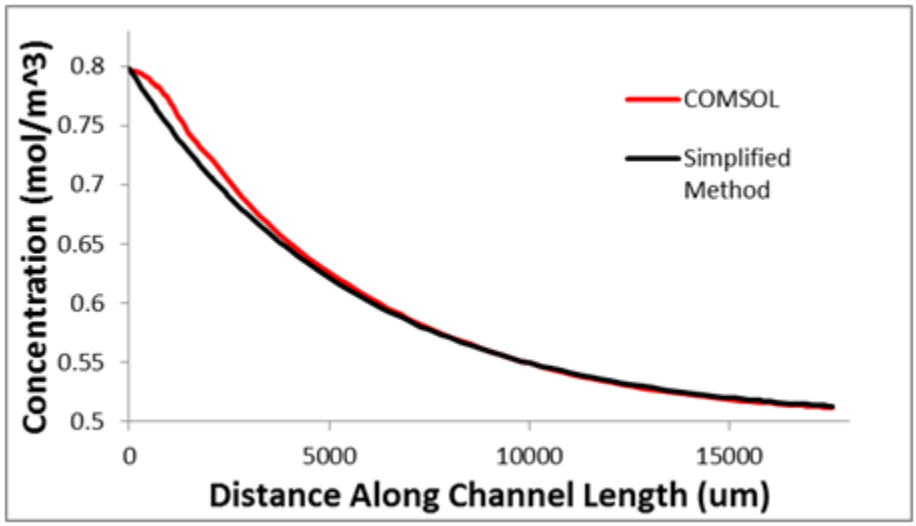

Figure 5-11. A comparison of the concentration profiles along the channel length obtained using COMSOL and the simplified method described here. This line profile corresponds to 1000 microns across the channel width, or 200 microns from the side wall with the highest concentration of the chemoeffector.

An example of these calculations is shown in Appendix B. Finally, the bacterium's position along the channel length is substituted for x and the exact concentration at that point can be found. This method eliminates the need for complex fluidic computations as a prerequisite for chemotaxis simulations.

Chapter 6: Discussion

6.1 Representative Results

When this flow-based gradient generator is free of issues, it may generate an observable chemotactic response, as shown in Fig. 6-1.

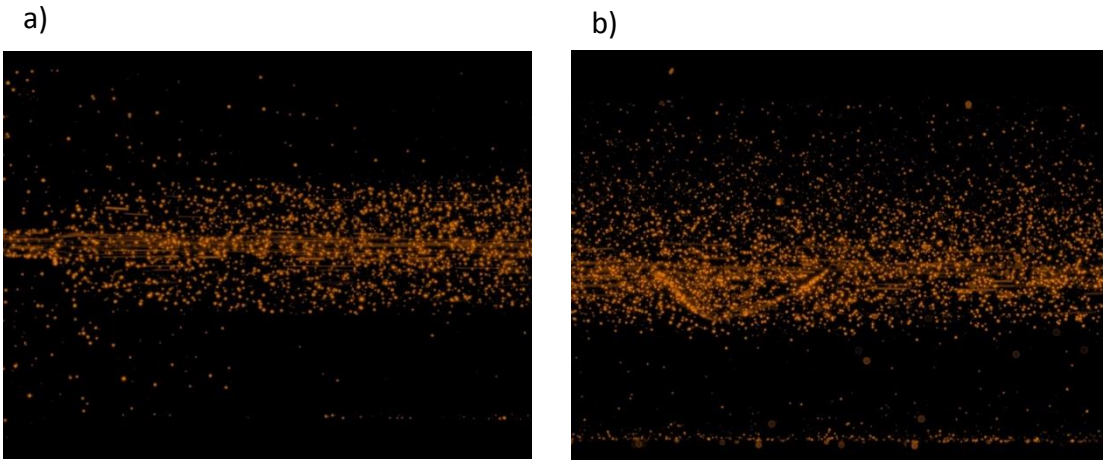

Figure 6-1. An example of how chemotaxis occurring a flow-based microfluidic gradient generator may appear, where a) is the beginning of the main channel where the cell inlet is joined, and b) is the end of the channel where the majority of chemotaxis would be completed.

However, the bacteria remains highly concentrated at the center of the channel. When the chemotactic response is quantified using ImageJ software to measure the fluorescent intensity across the channel width, as shown in Fig. 6-2, the chemotactic response is evident as a slight difference in the intensity of the fluorescence near the channel edges, but this difference is small relative to the intensity at the center of the channel.

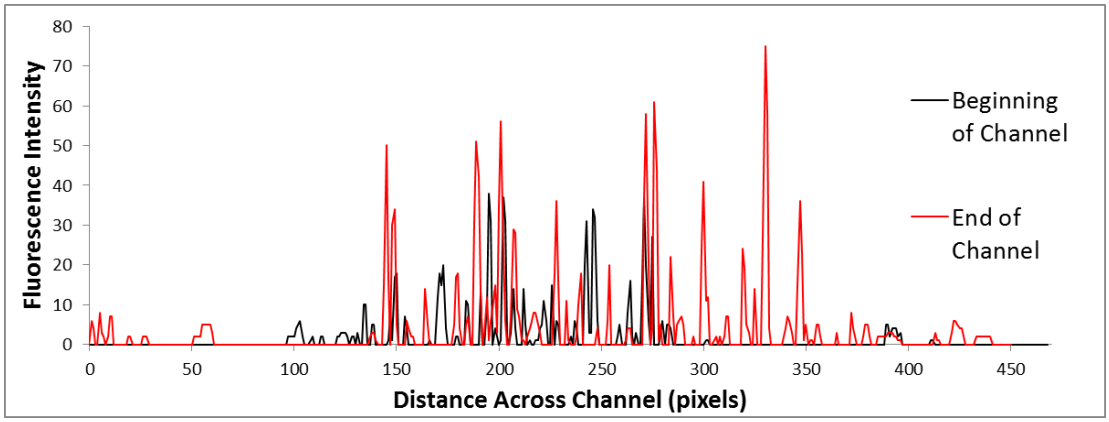

Figure 6-2. The corresponding ImageJ analysis of the fluorescence intensity of the images in Fig. 6-1. The differences in fluorescence intensity are represented as an increase in the number of peaks occurring on the side of the channel with a higher concentration of chemoeffector, while the cells at the beginning of the channel are more evenly distributed in the center.

Appendix C shows images and the corresponding ImageJ analyses that are more representative of what occurs in this device. Even though none of them display any observable chemotaxis, it is noteworthy that there is a large degree of variation of the distribution of the cells near the center of the channel. This seems to indicate that small variations in environmental factors or the sources of error that have been noted throughout this thesis can have a significant effect on what is observed in the device.

6.2 Summary of Key Findings

An examination of the fundamental principles of these devices, in conjunction with the known behavior and properties of *E. coli*, indicate that these platforms are not suitable for the study of bacterial chemotaxis, and that previously reported results may instead be the product of other factors. The effects of shear flow severely attenuate chemotactic response, and while shear can be minimized through decreasing the velocity at which solutions flow through the device, this in turn leads to more rapid gradient decay. Bacteria in a shallow gradient will exhibit a weaker

chemotactic response, and both the experimental results shown here and a review of the literature indicate that chemotaxis is not strongly apparent in any microfluidic gradient generators. However, this microfluidic gradient generator design is used in a wide variety of applications besides bacterial chemotaxis, and the detailed exploration of troubleshooting methods provided in this thesis may prove useful for future work in other fields.

6.3 Future Work

The study of bacterial chemotaxis is still in need of a platform that meets several requirements:

(1) Simple, rapid, inexpensive fabrication

(2) Simple and repeatable operation

(3) Minimal sources of error or need for troubleshooting

(4) Precise manipulation of chemical gradients

(5) Temporal tracking of individual bacteria and bacteria populations

(6) Easily visible chemotaxis

At the time of writing, microfluidic gradient generators that subject the bacteria to a stable, non-flowing environment seem to represent the best solution. However, future work may examine whether the static gradient generation of flow-based gradient generators can be harnessed through a three-dimensional microfluidic structure, by integrating the bacteria into adjacent chambers. through which diffusion can occur. This represents an increase in complexity of both fabrication and operation, but there may not be a “catch-all” platform for the study of bacterial chemotaxis. Instead, researchers may need to determine whether they need rapid

generation of simple results, in which case the chemotaxis assays described in 1.4.1 may be used, or if they are testing a more complex chemotactic response, in which case they could use one of the many microfluidic platforms described in the literature.

Further work is needed to expand on the interactions of bacteria flagella with the walls of a microchannel. The experiment described in 5.1.2 is an adequate starting point, a more systematic evaluation that incorporates the effects of different materials (glass vs. PDMS), varying flow rates, bacteria dispersed in different solutions, and varying channel dimensions could more accurately characterize the significance of this effect. Additionally, these tests should be performed with different strains of bacteria with mutations, namely mutations to make strains non-motile or aflagellated. When compared with wild-type, these strains allows for the elimination of any contributing effects from bacterial swimming by observing the flagellated but non-motile strain, and then the determination of whether surface interactions are a product of flagellar interactions or body interactions, by observing the aflagellated strain.

While there are several papers documenting simulations of bacterial chemotaxis in shear flow, almost all of these papers disregard the effects of shear on the flagella, even though research has shown that this can further attenuate the chemotactic response and alter swimming trajectories[41–43]. Additionally, the simulations all disregard the effects of shear during tumbling events, although the shear can significantly displace a bacterium when it is not exerting a directional swimming force. Future simulations of bacterial chemotaxis in flowing environments should incorporate these factors, as well as use updated models for the chemotactic response of bacteria to ensure accuracy of the simulated chemotactic response.

Appendix A

Position and Flow Rate	Boltzmann Curve Fit Equation
Beginning of Channel 1 μL/min	$y = 0.86653 + \frac{-0.73524}{1 + e^{\left[\left(\frac{1200(x+\frac{W}{2})}{W} - 600.05929\right) \Big/ 74.4636\right]}}$
End of Channel 1 μL/min	$y = 0.71996 + \frac{-0.43715}{1 + e^{\left[\left(\frac{1200(x+\frac{W}{2})}{W} - 602.70882\right) \Big/ 147.56036\right]}}$
Beginning of Channel 0.1 μL/min	$y = 0.79796 + \frac{-0.59647}{1 + e^{\left[\left(\frac{1200(x+\frac{W}{2})}{W} - 604.66096\right) \Big/ 39.66651\right]}}$
End of Channel 0.1 μL/min	$y = 0.51376 + \frac{-0.03076}{1 + e^{\left[\left(\frac{1200(x+\frac{W}{2})}{W} - 584.62101\right) \Big/ 170.8525\right]}}$

Appendix B

Example of solving for concentration at bacterium position of 800 microns across the channel width (which corresponds to 200 microns in the equation, where the center is at 600 microns and is normalized to zero), and 7000 microns down the channel length, when flow rate=0.1 μL/min.

Beginning of channel:

$$y = 0.79796 + \frac{-0.59647}{1 + e^{\left[\left(\frac{1200(x+\frac{W}{2})}{W} - 604.66096\right) \Big/ 39.66651\right]}}$$

Substitute in $x = 200$, $W = 1200$:

$$y_1 = 0.794$$

Repeating for the equation for the end of the channel:

$$y = 0.51376 + \frac{-0.03076}{1 + e^{\left[\left(\frac{1200(x+\frac{W}{2})}{W} - 584.62101\right) \Big/ 170.8525\right]}}$$

$$y_2 = 0.507$$

The equation along the channel width is of the form:

$$y = Ae^{x/B} + C$$

In this device, $C = 0.5$, the concentration at the center of the channel (which corresponds to $x = 0$). Thus, it is possible to solve for A and B.

$$y_1 = Ae^0 + 0.5 = A + 0.5$$

$$A = y_1 - 0.5$$

$$y_2 = Ae^{x_2/B} + 0.5$$

Combining the two equations:

$$y_2 = (y_1 - 0.5)e^{x_2/B} + 0.5$$

$$\frac{y_2 - 0.5}{y_1 - 0.5} = e^{x_2/B}$$

$$\ln\left(\frac{y_2 - 0.5}{y_1 - 0.5}\right) = \frac{x_2}{B}$$

$$B = \frac{x_2}{\ln\left(\frac{y_2 - 0.5}{y_1 - 0.5}\right)}$$

These equations are a general form for A and B which can be used for other device dimensions and points along the channel width. The final equation is then:

$$y = (y_1 - 0.5)e^{\left[x \Big/ \frac{x_2}{\ln\left(\frac{y_2 - 0.5}{y_1 - 0.5}\right)}\right]} + 0.5$$

In this scenario, where $x_2 = 17700$ (as determined by where the line profiles were originally taken), $y_1 = 0.702$, and $y_2 = 0.476$, the final equation would then be:

$$y = 0.294e^{(x/-4735.57)} + 0.5$$

Finally, to calculate the concentration at the original point, the position of the bacterium along the channel length, 7000 microns, can be substituted for x, to yield

$$\text{Concentration} = 0.567 \text{ mM}$$

The concentration at this point obtained from a COMSOL simulation is 0.557 mM, thus the solution has 1.8% error at this point. The deviation between the method described here and the results obtained computationally with COMSOL is highest at the beginning of the channel, and at the side walls of the channel width.

Appendix C

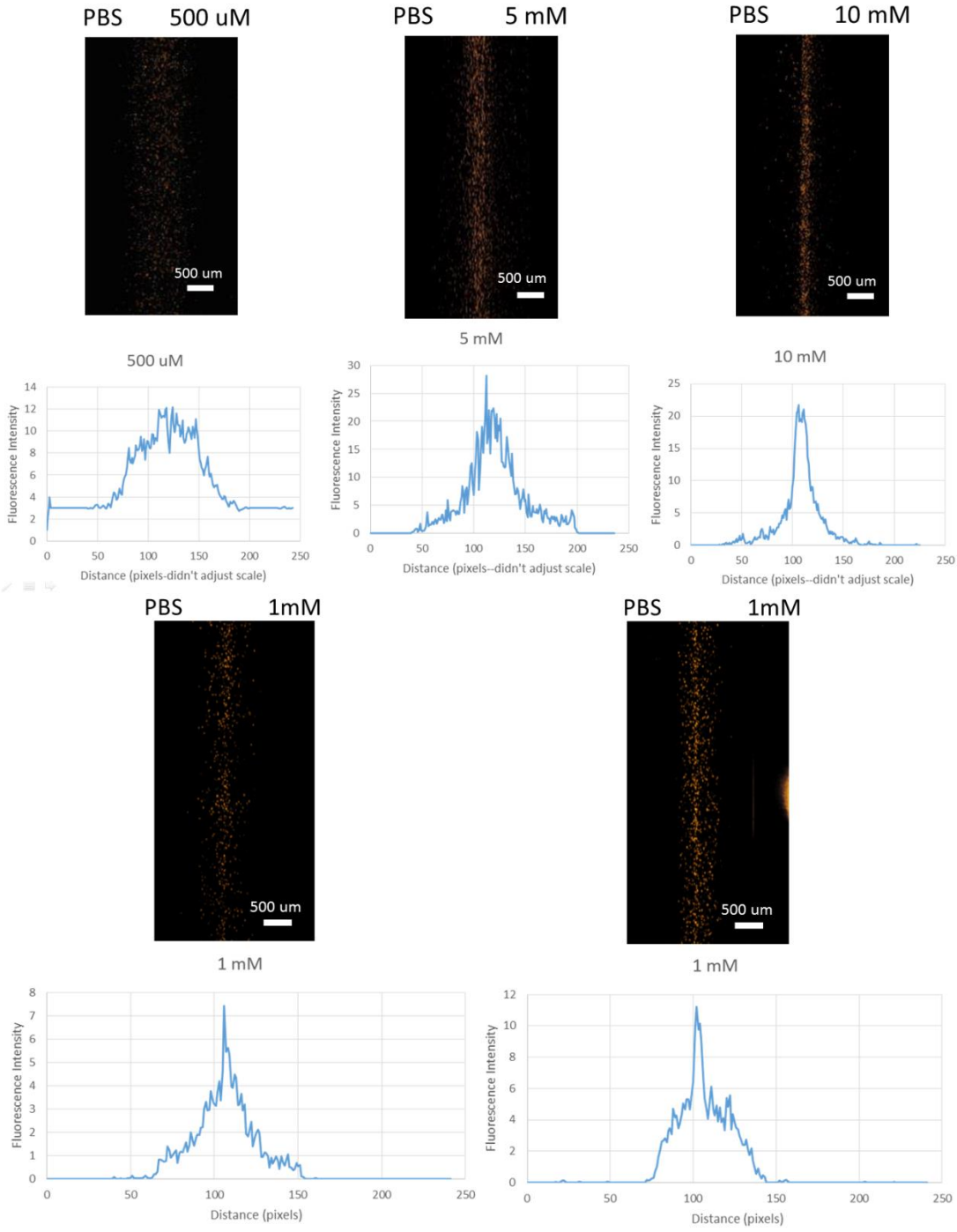
PBS
500 uM
500 um
PBS
5 mM
500 um
PBS
10 mM
500 um
500 uM
Fluorescence Intensity
Distance (pixels-didn't adjust scale)
5 mM
Fluorescence Intensity
Distance (pixels--didn't adjust scale)
10 mM
Fluorescence Intensity
Distance (pixels--didn't adjust scale)
PBS
1mM
500 um
PBS
1mM
500 um
1 mM
Fluorescence Intensity
Distance (pixels)
1 mM
Fluorescence Intensity
Distance (pixels)

Bibliography

1. Adler, J. Chemotaxis in Bacteria. *Science (80-.).* **153,** 708–716 (1966).

2. Macnab, R. M. & Koshland, D. E. The Gradient-Sensing Mechanism in Bacterial Chemotaxis. *Proc. Natl. Acad. Sci.* **69,** 2509–2512 (1972).

3. Tso, W. & Adler, J. Negative Chemotaxis in Escherichia coli. *J. Bacteriol.* **118,** 560 (1974).

4. Kort, E. N. & Larsen, S. H. Methylation of a membrane protein involved in bacterial chemotaxis. *Proc. Natl. Acad. Sci.* **72,** 3939–3943 (1975).

5. Min, T. L. *et al.* High-resolution, long-term characterization of bacterial motility using optical tweezers. *Nat. Methods* **6,** 831–5 (2009).

6. Greenfield, D. *et al.* Self-organization of the Escherichia coli chemotaxis network imaged with super-resolution light microscopy. *PLoS Biol.* **7,** e1000137 (2009).

7. Ishihara, A., Segall, J. E., Block, S. M. & Berg, H. C. Coordination of flagella on filamentous cells of Coordination of Flagella on Filamentous Cells of Escherichia coli. *J. Bacteriol.* **155,** 228 (1983).

8. Grebe, T. W. & Stock, J. Bacterial chemotaxis: The five sensors of a bacterium. *Curr. Biol.* **8,** R154–R157 (1998).

9. Sourjik, V. & Berg, H. C. Localization of components of the chemotaxis machinery of Escherichia coli using fluorescent protein fusions. *Mol. Microbiol.* **37,** 740–751 (2000).

10. Parkinson, J. S. Signal transduction schemes of bacteria. *Cell* **73,** 857–871 (1993).

11. Levit, M. N., Liu, Y. & Stock, J. B. Stimulus response coupling in bacterial chemotaxis : receptor dimers in signalling arrays. *Mol. Microbiol.* **30,** 459–466 (1998).

12. Adler, J., Hazelbauer, G. L. & Dahl, M. M. Chemotaxis Toward Sugars in Escherichia coli. *J. Bacteriol.* **115,** 824–847 (1973).

13. Mesibov, R. & Adler, J. Chemotaxis Toward Amino Acids in Escherichia coli. *J. Bacteriol.* **112,** 315 (1972).

14. Antúnez-Lamas, M. *et al.* Role of motility and chemotaxis in the pathogenesis of Dickeya dadantii 3937 (ex Erwinia chrysanthemi 3937). *Microbiology* **155,** 434–442 (2009).

15. Qin, Y., Yan, Q., Su, Y., Li, H. & Zou, W. Disruption of chemotaxis-related genes affects multiple cellular processes and the virulence of pathogenic Vibrio harveyi. *Acta Oceanol. Sin.* **32,** 55–60 (2013).

16. Sweeney, E. & Guillemin, K. A gastric pathogen moves chemotaxis in a new direction. *MBio* **2,** 1–3 (2011).

17. Purcell, E. M. Life at Low Reynolds Number. *Am. J. Phys.* **45,** 3–11 (1977).

18. Mishler, D. M., Topp, S., Reynoso, C. M. K. & Gallivan, J. P. Engineering Bacteria To Recognize And Follow Small Molecules. *Curr. Opin. Biotechnol.* **21,** 653–656 (2010).

19. Hwang, I. Y. *et al.* Reprogramming Microbes to Be Pathogen-Seeking Killers. *ACS Synth. Biol.* (2013). doi:10.1021/sb400077j

20. Sinha, J., Reyes, S. J. & Gallivan, J. P. Reprogramming bacteria to seek and destroy an herbicide. *Nat. Chem. Biol.* **6,** 464–70 (2010).

21. Wu, H.-C. *et al.* Autonomous bacterial localization and gene expression based on nearby cell receptor density. *Mol. Syst. Biol.* **9,** 636 (2013).

22. Adler, J. A Method for Measuring Chemotaxis and Use of the Method to Determine Optimum Conditions for Chemotaxis by Escherichia coli. *J. Gen. Microbiol.* **74,** 77–91 (1973).

23. Brown, D. a. & Berg, H. C. Temporal Stimulation of Chemotaxis in Escherichia coli. *Proc. Natl. Acad. Sci.* **71,** 1388–1392 (1974).

24. Nelson, R. D., Quie, P. G. & Simmons, R. L. Chemotaxis Under Agarose : A New and Simple Method for Measuring Chemotaxis and Spontaneous Migration of Human Polymorphonuclear Leukocytes and Monocytes. *J. Immunol.* **115,** 1650–1656 (1975).

25. Wolfe, A. J. & Berg, H. C. Migration of bacteria in semisolid agar. *Pro* **86,** 6973–6977 (1989).

26. Li, J., Go, A. C., Ward, M. J. & Ottemann, K. M. The chemical-in-plug bacterial chemotaxis assay is prone to false positive responses. *BMC Res. Notes* **3,** (2010).

27. Kanungpean, D., Kakuda, T. & Takai, S. False Positive Responses of Campylobacter jejuni when Using the Chemical-In-Plug Chemotaxis Assay. *J. Vet. Med. Sci.* **73,** 389–391 (2011).

28. Choudhury, D. *et al.* Fish and Chips: a microfluidic perfusion platform for monitoring zebrafish development. *Lab Chip* **12,** 892–900 (2012).

29. Tian, X., Wang, S., Zhang, Z. & Lv, D. Rat bone marrow-derived Schwann-like cells differentiated by the optimal inducers combination on microfluidic chip and their functional performance. *PLoS One* **7,** 1–11 (2012).

30. Lou, X. *et al.* A high-throughput photodynamic therapy screening platform with on-chip control of multiple microenvironmental factors. *Lab Chip* **14,** 892–901 (2014).

31. Diao, J. *et al.* A three-channel microfluidic device for generating static linear gradients and its application to the quantitative analysis of bacterial chemotaxis. *Lab Chip* **6,** 381–8 (2006).

32. Wang, L., Hashimoto, Y., Tsao, C.-Y., Valdes, J. J. & Bentley, W. E. Cyclic AMP (cAMP) and cAMP receptor protein influence both synthesis and uptake of extracellular autoinducer 2 in Escherichia coli. *J. Bacteriol.* **187,** 2066–76 (2005).

33. Englert, D. L., Manson, M. D. & Jayaraman, A. Flow-based microfluidic device for quantifying bacterial chemotaxis in stable, competing gradients. *Appl. Environ. Microbiol.* **75,** 4557–64 (2009).

34. Stone, H. A. in *C. Biotechnol.* (Lee, H., Ham, D. & Westervelt, R. M.) 5–30 (Springer Science & Business Media, LLC, 2007).

35. Abadian, P. N. & Goluch, E. D. Surface plasmon resonance imaging (SPRi) for multiplexed evaluation of bacterial adhesion onto surface coatings. *Anal. Methods* **7,** 115–122 (2015).

36. Darnton, N. C., Turner, L., Rojevsky, S. & Berg, H. C. On torque and tumbling in swimming Escherichia coli. *J. Bacteriol.* **189,** 1756–64 (2007).

37. Vladimirov, N., Løvdok, L., Lebiedz, D. & Sourjik, V. Dependence of Bacterial Chemotaxis on Gradient Shape and Adaptation Rate. *PLoS Comput. Biol.* **4,** (2008).

38. Vladimirov, N. Multiscale Modeling of Bacterial Chemotaxis. 1–115 (2009).

39. Sourjik, V. & Berg, H. C. Receptor sensitivity in bacterial chemotaxis. *Proc. Natl. Acad. Sci.* **99,** 123–127 (2002).

40. Bearon, R. N. & Pedley, T. J. Modelling run-and-tumble chemotaxis in a shear flow. *Bull. Math. Biol.* **62,** 775–91 (2000).

41. Locsei, J. T. & Pedley, T. J. Run and tumble chemotaxis in a shear flow: the effect of temporal comparisons and other complications. *Bull. Math. Biol.* **71,** 1089–1116 (2009).

42. Tournus, M., Kirshtein, A., Berlyand, L. V & Aranson, I. S. Flexibility of bacterial flagella in external shear results in complex swimming trajectories. *Proc. R. Soc. London A* **12,** 1–11 (2014).

43. Rusconi, R., Guasto, J. S. & Stocker, R. Bacterial transport suppressed by fluid shear. *Nat. Phys.* **10,** 212–217 (2014).

44. Molaei, M., Barry, M., Stocker, R. & Sheng, J. Failed Escape: Solid Surfaces Prevent Tumbling of *Escherichia coli*. *Phys. Rev. Lett.* **113,** 068103 (2014).